Pressure Distribution and Flow Rate Behavior in Continuous-Casting Slide-Gate Systems: PFSG

HAMED OLIA, HYUNJIN YANG, SEONG-MOOK CHO, MINGYI LIANG, LIPSA DAS, and BRIAN G. THOMAS

Quantifying the pressure distribution and flow rate in the metal delivery system from the tundish to the mold is important to understand nozzle clogging due to air aspiration, argon bubble size, and other important phenomena in continuous casting of steel. A one-dimensional pressure energy model, PFSG, is presented here to calculate pressure distribution and flow rate in slide-gate nozzle systems for argon-molten steel flow systems including argon gas expansion by solving a system of Bernoulli equations. PFSG is a user-friendly MATLAB-based software package with an intuitive Graphical User Interface capable of inverse solutions that enables users to conduct parametric studies in seconds. The model predictions is verified with computational fluid dynamics simulations and validated with plant measurements and water model measurements, with errors of less than 6 pct. The verified and validated PFSG model is then applied to investigate the effect of different casting conditions on the flow rate and pressure distribution. For a given slide gate opening, the flow rate increases with increasing distance from the tundish level to the mold level, increasing SEN diameter, and decreasing argon gas injection rate. The slide-gate opening fraction that produces the minimum pressure is almost independent of casting conditions, except for SEN bore diameter. This critical opening fraction, which is most detrimental for air aspiration, increases from 50 to 70 pct with increasing SEN diameter by 13 pct for the system studied. The minimum pressure worsens (decreases) with increasing tundish height and/or nozzle bore diameter.

https://doi.org/10.1007/s11663-022-02476-8

I. INTRODUCTION

THE pressure distribution in continuous-casting flow control systems from the tundish into the upper tundish nozzle (UTN), past the slide gate flow control, into the submerged entry nozzle (SEN), through the ports and finally up to the top surface in the mold is important for many reasons. Firstly, it governs the flow rate (and corresponding casting speed) in this gravity-driven process. Secondly, it is crucial to the minimum pressure beneath the slide gate, where air aspiration, reoxidation, and nozzle clogging may occur.[1,2] When pressure inside the nozzle drops below atmospheric pressure, air may be drawn into the nozzle through any cracks, leaks at joints, or permeable gas flow through the porous refractory.[1–3] The oxygen and nitrogen can react with dissolved alloy elements in the molten steel to form oxide and nitride inclusions, which may adhere to the nozzle walls as clogging, or become entrained into the final product as inclusion defects.[4,5]

Clogging may occur at different places inside the nozzle, depending on the formation mechanism.[1,3,4] Air aspiration tends to cause clogging near joints or cracks in the refractory walls, while flow separation leads to clogging due to exogenous inclusion buildup below the slide-gate and top of the port outlets.[1–3] Clogging is detrimental because (1) it alters the effective nozzle geometry, decreasing the cross sectional area thus requiring more frequent nozzle replacement[4,5] (2) it agglomerates inclusions into larger, more detrimental particles if the clog partially breaks away, and 3) it causes flow variations, leading to more severe level fluctuations in the mold,[6] which ultimately increases sliver defects in the final product.[7–9]

HAMED OLIA, MINGYI LIANG and LIPSA DAS are with the Department of Mechanical Engineering, Colorado School of Mines, 1610 Illinois Street, Golden, CO 80401. HYUNJIN YANG is with the Process Metallurgy Department, SWERIM AB Aronstorpsvagen 1, 97 437, Lulea, Sweden. SEONG-MOOK CHO is with the Department of Metallurgical Engineering, Pukyong National University, 45, Yongso-ro, Nam-gu, Busan 48513, Republic of Korea. BRIAN G. THOMAS is with the Department of Mechanical Engineering, Colorado School of Mines and also with the Department of Mechanical Science and Engineering, University of Illinois at Urbana-Champaign, 1206 West Green Street, Urbana, IL 61801. Contact e-mail: bgthomas@mines.edu

Manuscript submitted October 19, 2021; accepted February 15, 2022.

Article published online March 17, 2022.

For these reasons, it is beneficial to minimize pressure drops below atmospheric pressure inside the nozzle. An alternative suggestion to reduce air aspiration is to surround the slide gate with a vacuum chamber,[10] but this is not feasible in practice. A common commercial practice is to introduce argon into the slide gate region, in order to encourage the aspiration of argon instead of air or to actively inject argon gas. Argon may act in several ways to lessen clogging, which are reviewed elsewhere.[1,2,4] Finally, the most important and least expensive method to minimize reoxidation from pressure drops is to optimize the nozzle geometry[5] according to the casting conditions, such as tundish height, casting speed, slide gate opening, and argon gas injection rate.

Only a few previous studies using validated models have been undertaken to understand the pressure distribution in a slide-gate flow control system as a function of the system geometry and casting conditions. These models employed a Bernoulli energy-balance approach,[4,11,12] computational fluid dynamics (CFD) models,[13,14] or a curve fit of polynomial functions.[1] The results indicated that the combined effects of fluid control systems (slide-gate opening or stopper rod opening), casting speed, nozzle geometry (nozzle length and diameter), argon gas injection, tundish height (depth or level of molten steel inside tundish) are required to calculate the pressure distribution as well as system flow rate. Bai *et al*.[1] found that a near-vacuum situation might appear in the slide-gate region for small slide-gate opening. They found that injection of argon gas can alleviate the negative pressure problem, and quantified how much argon is needed for different nozzle diameters and casting conditions. For most conditions, the required argon is unfeasibly high.

Liu and Thomas proposed a 1D analytical model, based on the Bernoulli energy-balance approach, to relate stopper rod position and flow rate.[12] Their parametric studies quantify how system flow rate changes with increasing clogging and eventually requires the stopper rod to open further to maintain the flow rate. Recently, Yang *et al*.[2] improved this analytical approach to quantify pressure distribution and flow rate in slide gate metal delivery system. Pressure distributions were shown for different SEN diameters for a typical slab casting operation, assuming incompressible flow. Decreasing SEN diameter was shown to lessen the problem of negative pressure for a given casting speed and argon gas flow rate.

Many previous computational models of multiphase flow in continuous casting of steel have been developed and applied to investigate fluid flow in the nozzle[14,15] and/or mold/strand,[16–18] including the effect of argon gas injection, which are reviewed elsewhere.[19,20] The few that show pressure distributions[1,2,13,14,21–23] confirm that pressure in the gap region in both slide gate[1,2,14,21–23] and stopper rod[13,23] flow control systems can easily drop below atmospheric pressure. However, parametric studies are limited and no previous model has considered the effect of compressibility of the argon gas on flow and pressure inside the nozzle even though this effect has been shown to be very important in closely-related systems.[24,25]

The present work introduces a new computationally-efficient modeling package for calculating Pressure distribution and Flow rate within Slide Gate flow delivery systems: PFSG. This software package improves on the model developed by Yang *et al*.,[2] and features a user-friendly Graphical User Interface (GUI) with other enhancements, such as inverse-modeling capabilities, non-circular nozzle cross sections, and clogging resistances which vary with location. PFSG also includes the effect of gas compressibility, which varies the argon flow rate locally, due to pressure variations in the flow system. Parametric studies are conducted with PFSG to investigate the combined effects of tundish height, SEN submergence depth, casting speed, gas injection rate, and nozzle geometry on slide-gate opening, flow rate, and pressure distribution in the nozzle.

II. PFSG MODEL DESCRIPTION

A new model based on the Bernoulli energy-balance approach, PFSG, has been developed to calculate pressure distribution and flow rate in slide-gate flow-control systems for continuous casting of steel slabs. The program features a user-friendly graphical interface and is already in use at several steel plants. The PFSG model calculates flow and pressure, starting in the tundish, through the UTN, slide-gate plates, SEN, and ending at the top surface level in the mold. Pressure is calculated at different points in the metal delivery system as a function of geometry and process conditions, including the flow rate, slide gate opening, argon gas injection rate, fluid density, UTN and SEN absolute roughness, and possible clogging. The model equations are solved with MATLAB[26] and are presented in the next section, followed by a description of the inputs and outputs.

A. *Pressure-Energy Model Equations*

The PFSG model solves a one-dimensional system of pressure–energy balance equations for fluid flow, including kinetic energy, potential energy, and turbulent dissipation pressure/energy losses, based on a Bernoulli approach.[2] General analytical expressions are obtained for the pressure/energy loss between 10 selected points distributed vertically in the slide-gate system (shown in Figure 1), which follow the main streamline of molten steel flow from the tundish top surface through the UTN, slide gate, SEN, ports, and to the mold level.[2] Pressure is calculated at each point in the system by:

$$P_x = P_{x+1} + \rho_m g h_{x+1} - \rho_m g h_x + \frac{1}{2}\rho_m V_{x+1}^2 - \frac{1}{2}\rho V_x^2 + \sum \Delta P_L \quad [1]$$

where P_x is gauge pressure of point x [Pa], ρ_m is mixture fluid density [kg/m^3], V_x is velocity at point x [m/s], h_x is the height associated with point x [m], and g is gravitational acceleration [9.81 m/s^2]. With this form of the equation, the velocities must be calculated first from the system flow rate. Boundary conditions of 1 atm pressure are applied at the top surfaces of the tundish and the mold level, Finally, the pressure energy loss terms, $\sum \Delta P_L$, [Pa] are explained in Section II–C, and depend on the geometric details between each pair of points.

Most of these equations are given by Yang *et al.*,[2] but several terms include new improvements.

B. *Velocity and Area Calculations*

Velocity at each point in the PFSG model, V_x, [m/s] is calculated from the system flow rate as follows:

$$V_x = \frac{Q}{A_{\text{eff},x}} \quad [2]$$

where Q is the liquid (water or steel) flow rate [m^3/s], and $A_{\text{eff},x}$ is the effective area of the local cross section [m^2] considering air or argon gas injection, as discussed in the next section.

1. *Effective area calculations*

With no argon gas injection, A_x is the area of the cross section of the nozzle at any given point (x) in the model [m^2]. However, if argon gas is injected, then it will limit the effective area for molten steel flow according its volume fraction at point x, α_x, which varies with vertical position in the model system according to:

$$\alpha_x = 1 - \frac{Q}{Q_{\text{gas},x} + Q} \quad [3]$$

where $Q_{\text{gas},x}$ is the flow rate of the "hot" (*i.e.* at molten steel temperature, $T_{\text{hot}} =$ 1823 K) argon gas at point x [m^3/s] and is calculated as follows:

$$Q_{\text{gas},x} = SLPM \times \frac{P_{\text{atm}}}{P_{\text{atm}} + \left(\frac{P_{x+1}+P_x}{2}\right)} \times \frac{T_{\text{hot}}}{T_\infty} \times \frac{0.001}{60} \quad [4]$$

where $SLPM$ is the flow rate of the "cold" (*i.e.* at ambient temperature T_∞ = 298 K) argon gas injected in standard liters per minute, P_{atm} is the standard (atmospheric) pressure 101 kPa, and P_{x+1} is gauge pressure at point $x+1$ [kPa] (previously calculated downstream pressure). Therefore, the effective cross section area for steel flow at point x, $A_{\text{eff},x}$, and the mixture density between two points are expressed as:

$$A_{\text{eff},x} = A_x \times (1 - \alpha_x) \quad [5]$$

$$\rho_m = \rho_L \times (1 - \alpha_x) \quad [6]$$

where A_x is the cross section area at point x, according to the nozzle geometry [m^2] and ρ_L is liquid density [kg/m^3].

For the UTN entry, UTN exit, upper plate, middle plate, and lower plate, the cross section is considered to be circular, which can be calculated as follows:

$$A_x = \frac{\pi}{4} D_x^2 \quad [7]$$

where D_x is the diameter of that place, x, down the nozzle [m]. At other vertical locations down the nozzle system, the area and perimeter are required inputs to define the geometry for more generality, and are used to calculate $D_{h,x}$, the equivalent hydraulic diameter [m], as follows:

$$D_{h,x} = \frac{4A_x}{p_x} \quad [8]$$

where p_x is the perimeter at that location, x [m]. Furthermore, for a bifurcated port, if the port area is greater than half of the SEN area, it is set back down to half of the SEN area, because the jet exiting the port cannot expand fast enough to change its area significantly, so the rest of the area, in the upper port, typically has negligible net outward flow.[1,2]

2. *Gap area calculation*

The minimum cross-section area of the gap formed in the slide gate region, A_{gap}, [m^2] is calculated as follows[27]:

$$A_{\text{gap}} = R_1^2 \arccos\left(\frac{R_1^2 - R_2^2 + d^2}{2R_1 d}\right) + R_2^2 \arccos\left(\frac{R_2^2 - R_1^2 + d^2}{2R_2 d}\right) - \frac{1}{2}\sqrt{4R_1^2 d^2 - \left(R_1^2 - R_2^2 + d^2\right)^2} \quad [9]$$

In which:

$$D = \min\left(D_{\text{slide}}, D_p\right), \quad d = \frac{D_{\text{slide}} + D_p}{2} - Df_L \quad [10]$$

$$R_1 = \frac{\max\left(D_{\text{slide}}, D_p\right)}{2}, \quad R_2 = \frac{\min\left(D_{\text{slide}}, D_p\right)}{2} \quad [11]$$

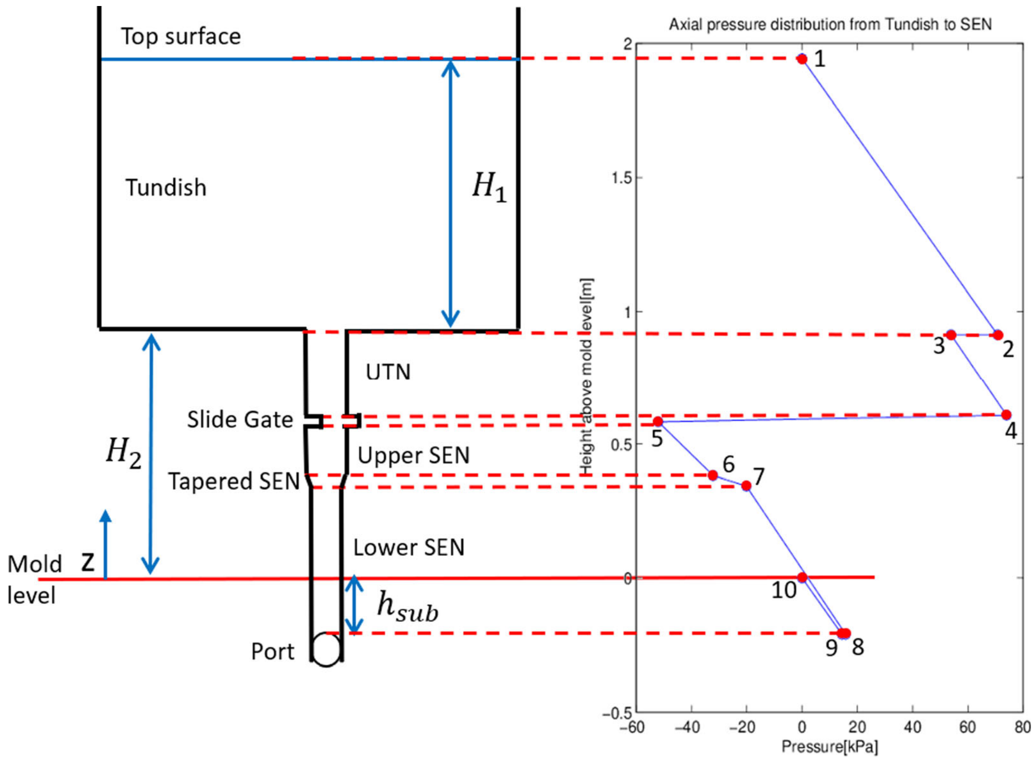

Fig. 1—Example pressure distribution for all 10 points in slide-gate metal delivery system (Nozzle 1 conditions).

where D_{slide} is the diameter of the sliding middle plate hole, D_{p} is the diameter of the lower/upper fixed plates of the slide gate in [m], and f_{L} is the linear slide gate opening fraction. Note that the lower and upper plates are assumed to have the same diameter.

C. *Pressure Losses*

The PFSG model incorporates pressure loss terms, $\sum \Delta P_{\mathrm{L}}$ in Eq. [1], between each pair of points in the system in Figure 1.

1. *Tundish liquid level to tundish floor (points 1 to 2)*

The top of the liquid level in the tundish is at atmospheric pressure, so P_1 is zero gauge pressure. This is the top boundary condition for the 1-D model. Between point 1 and the tundish floor exit to UTN (point 2) velocity is negligible and there are no pressure losses, so Eq. [1] simplifies to the potential energy term for the classic hydrostatic pressure gain:

$$P_2 = \rho_{\mathrm{L}} g (h_1 - h_2) \quad [12]$$

This equation is also used between points 9 and 10, by replacing $(h_1 - h_2)$ with $(h_9 - h_{10})$. Similarly, the liquid level in the mold is at atmospheric pressure which defines the bottom boundary condition of the model ($P_{10} = 0$).

2. *Tundish floor to UTN region (points 2 to 3)*

When flow exits the tundish bottom into the UTN, it experiences a sudden contraction in area which causes a pressure loss that depends on the decrease in area, $P_{\mathrm{L,tun}}$, [Pa] and is expressed as[28]:

$$\Delta P_{\mathrm{L,tun}} = \frac{1}{2} \rho_{\mathrm{L}} (V_{\mathrm{UTNr}})^2 \left(0.42 \left(1 - \frac{n \times A_{\mathrm{UTNr}}}{A_{\mathrm{tun}}} \right) \right) \quad [13]$$

where V_{UTNr} is fluid velocity just before UTN entry [m/s], A_{UTNr} is upper UTN surface area [m^2] in contact with tundish floor with curvature radius of r [m], A_{tun} is area of the tundish bottom [m^2], and n is the number of nozzles where flow exits the tundish bottom.

Additionally, $\Delta P_{\mathrm{L,two}}$ is considered to account for the pressure drop caused by possible argon gas injection[2]:

$$\Delta P_{\mathrm{L,two}} = \frac{1}{2} \rho_{\mathrm{m}} (V_{\mathrm{UTNa}})^2 T \quad [14]$$

where V_{UTNa} is fluid velocity at UTN entry [m/s]. The pressure loss constant caused by the argon gas injection, T, is calculated based on the argon gas volume needed to be displaced to overcome the buoyancy effect, Vol_{gas}, in order to account for argon flow inside the nozzle. This constant is calculated as:

$$T = \frac{2g Vol_{\mathrm{gas}}}{A_{\mathrm{UTNa}} (V_{\mathrm{UTNa}})^2} \quad [15]$$

where A_{UTNa} is the area of the UTN inlet, and Vol_{gas} is defined as:

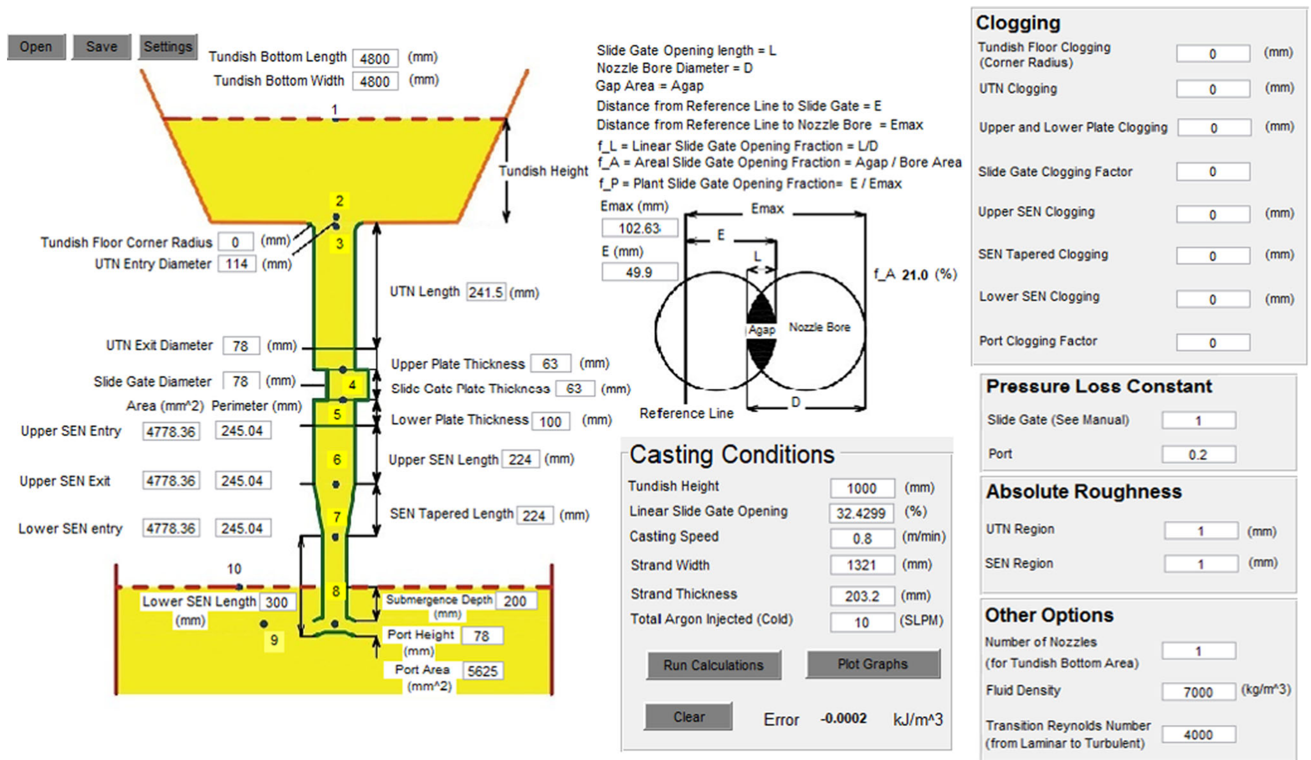

Fig. 2—PFSG V.3.2 user interface showing input data for Standard nozzle conditions.

$$Vol_{\text{gas}} = \sum Vol_x \alpha_x \qquad [16]$$

where Vol_x is the volume of the specific nozzle region (for example UTN). It should be noted that if argon gas is injected into the UTN, then all of the argon volume and gas fraction from the UTN up to the end of the lower SEN must be calculated and summed together to find Vol_x.

3. *UTN region (points 3 to 4)*

In this potentially tapered region, there are three pressure losses to sum between the top of the UTN and the upper plate at the bottom of the UTN, points 3 and 4: $\Delta P_{\text{Lf},3-4}$, $\Delta P_{\text{L,UTN}}$, and $\Delta P_{\text{L\_up}}$. The first, $\Delta P_{\text{Lf},3-4}$, is the pressure loss due to wall friction [Pa]:

$$\Delta P_{\text{Lf},3-4} = \frac{1}{8}\rho_{\text{m}} f_{\text{UTN}}\left[(V_{\text{UTNa}})^2 L_{\text{UTN}}\frac{(D_{\text{UTNa}}+D_{\text{UTNb}})(D_{\text{UTNa}}{}^2+D_{\text{UTNb}}{}^2)}{D_{\text{UTNb}}{}^4}+(V_{\text{UTNb}})^2 L_{\text{up}}\frac{(D_{\text{slide}}+D_{\text{p}})(D_{\text{slide}}{}^2+D_{\text{p}}{}^2)}{D_{\text{slide}}{}^4}\right] \qquad [17]$$

where f_{UTN} is the friction factor[28] in the UTN region, L_{UTN} and L_{up} are the UTN length and thickness of the upper plate [m], D_{UTNa} and D_{UTNb} are the UTN diameters at top and bottom [m], V_{UTNa} and V_{UTNb} are the corresponding flow velocities at UTN entry and exit [m/s]. A derivation for this equation for tapered pipes is provided in Appendix 1.

The second pressure loss inside the UTN, $\Delta P_{\text{L,UTN}}$, is the pressure loss due to gradual contraction or expansion[29] in the tapered UTN region [Pa], and is defined as follows, according to the UTN taper:

If $\boldsymbol{D_{UTNa} < D_{UTNb}}$ (*gradual expansion*)

$$\begin{cases} \Delta P_{\text{L,UTN}} = \frac{1}{4}\rho_{\text{m}} V_{\text{utna}}{}^2\left(2.6\sin\left(\frac{\theta}{2}\right)\right)\left(1-\frac{A_{\text{UTNa}}}{A_{\text{UTNb}}}\right)^2 \theta < 45\,\text{deg} \\ \Delta P_{\text{L,UTN}} = \frac{1}{4}\rho_{\text{m}} V_{\text{utna}}{}^2\left(1-\frac{A_{\text{UTNa}}}{A_{\text{UTNb}}}\right)^2 45^0 < \theta < 90\,\text{deg} \end{cases} \qquad [18]$$

If $D_{UTNa} \geq D_{UTNb}$ (*gradual contraction*)

$$\begin{cases} \Delta P_{\mathrm{L,UTN}} = \frac{1}{4}\rho_{\mathrm{m}} V_{\mathrm{utnb}}^2\left(1.6\sin\left(\frac{\theta}{2}\right)\right)\left(1-\frac{A_{\mathrm{UTNb}}}{A_{\mathrm{UTNa}}}\right)\theta < 45 \text{ deg} \\ \Delta P_{\mathrm{L,UTN}} = \frac{1}{4}\rho_{\mathrm{m}} V_{\mathrm{utnb}}^2\sqrt{\sin\left(\frac{\theta}{2}\right)}\left(1-\frac{A_{\mathrm{UTNb}}}{A_{\mathrm{UTNa}}}\right) 45 \text{ deg} < \theta < 90 \text{ deg} \end{cases} \quad [19]$$

where $\theta = 2 \times \arctan\left|\frac{D_{\mathrm{UTNa}} - D_{\mathrm{UTNb}}}{2L_{\mathrm{UTN}}}\right|$ [rad] and A_{UTNa} and A_{UTNb} are the corresponding area at UTN entry and exit [m^2].

The third pressure loss in the UTN, $\Delta P_{\mathrm{L\_up}}$, is due to sudden contraction or expansion[28] upon exit from the UTN into the upper plate [Pa], which may have different diameters:

If $D_p > D_{UTNb}$ (*sudden expansion*)

$$\Delta P_{\mathrm{L\_up}} = \frac{1}{2}\rho_{\mathrm{m}} V_{\mathrm{UTNb}}^2\left(1 - \frac{A_{\mathrm{UTNb}}}{A_{\mathrm{p}}}\right)^2 \quad [20]$$

If $D_p \leq D_{UTNb}$ (*sudden contraction*)

$$\Delta P_{\mathrm{L\_up}} = \frac{1}{2}\rho_{\mathrm{m}} V_{\mathrm{p}}^2\left(0.42\left(1 - \frac{A_{\mathrm{p}}}{A_{\mathrm{UTNb}}}\right)\right) \quad [21]$$

where V_{p} is fluid velocity at the upper plate in [m/s].

4. *Slide-gate region (points 4 to 5)*

In flowing through the slide gate, between points 4 and 5, four important pressure losses are considered, $\Delta P_{\mathrm{Lf,4-5}}$,$\Delta P_{\mathrm{C,sg}}$, $\Delta P_{\mathrm{L,sg}}$, and $\Delta P_{\mathrm{L,gate1}}$. The first, $\Delta P_{\mathrm{Lf,4-5}}$, is the wall friction [Pa], which is very small, but is included for completeness:

$$\Delta P_{\mathrm{Lf,4-5}} = \frac{1}{8}\rho_{\mathrm{m}} f_{\mathrm{UTN}} V_{\mathrm{p}}^2 h_{4-5}\frac{\left(D_{\mathrm{slide}} + D_{\mathrm{p}}\right)\left(D_{\mathrm{slide}}^2 + D_{\mathrm{p}}^2\right)}{D_{\mathrm{slide}}^4} \quad [22]$$

where f_{UTN} is the friction factor in the UTN, h_{4-5} the height difference between points 4 and 5 [m], D_{p} the diameter of the upper and lower plates [m], which are assumed to match, V_{p} is the flow velocity through the upper/lower plates [m/s].

The second pressure loss in the slide gate, $\Delta P_{\mathrm{C,sg}}$, is due to clogging as is treated as a pressure loss in the form of a kinetic energy change as follows:

$$\Delta P_{\mathrm{C,sg}} = \frac{1}{2}\rho_{\mathrm{m}} C_{\mathrm{sg}} V_{\mathrm{p}}^2 \quad [23]$$

where C_{sg} is the clogging coefficient of the slide gate which can be input (settings menu in Figure 2) or left blank, (to default to 0 for no clogging).

The third pressure loss in the slide gate, $\Delta P_{\mathrm{L,sg}}$, is due to restriction of the flow [Pa]:[2]

$$\Delta P_{\mathrm{L,sg}} = \frac{1}{2}\zeta\rho_{\mathrm{m}} V_{\mathrm{p}}^2\left(\frac{A_{\mathrm{p}}}{v A_{\mathrm{gap}}} - 1\right)^2 \quad [24]$$

where v is an empirical coefficient which is defined as[30]:

$$v = 0.63 + 0.37\left(\frac{A_{\mathrm{gap}}}{A_{\mathrm{sg}}}\right)^3 \quad [25]$$

where ζ is a slide gate pressure loss constant (introduced here to adjust the pressure drop due to flow passing through the slide gate), A_{gap} area of gap [m^2], and A_{sg} area of slide gate [m^2]. Although it is recommended to keep ζ equal to 1, this coefficient can be changed to calibrate the model if there are experimental measurements that the calculated pressure distribution by PFSG with $\zeta = 1$ does not match. To facilitate calibration, the user can leave the value of ζ blank in the Settings menu and let the inverse-modeling capability of PFSG calculate the value needed to match a given set of geometry and casting conditions.

Finally, the fourth pressure loss in the slide gate, $\Delta P_{\mathrm{L,gate\_1}}$, is due to sudden contraction or expansion at the transition between the lower part of the upper plate and the slide-gate middle-plate circular opening hole [Pa], and depends on the velocity of fluid in the gap as well as slide gate opening circular area. For a sudden expansion, the expression is the same as Eq. [20], changing V_{UTNb} to $\gamma\ V_{\mathrm{gap}}$, where γ is a velocity correction factor due to turbulent flow in the slide-gate region, as explained elsewhere[2] and V_{gap} is the velocity in the gap. Also, A_{UTNb} is replaced with A_{p} (slide-gate middle plate hole area [m^2]), and A_{p} is changed to A_{sg} (lower/upper plate area [m^2]). For a sudden contraction, the expression is Eq. [21], replacing V_{p} with $\gamma\ V_{\mathrm{gap}}$, A_{p} with A_{sg} *and* A_{UTNb} with A_{p}.

5. *Slide-gate and upper SEN region (points 5 to 6)*

In this potentially tapered region, four pressure loss terms are considered due to different geometry. The first term, $\Delta P_{\mathrm{Lf,5-6}}$, wall friction [Pa], is between points 5 and 6, and is similar to Eq. [17] replacing $\gamma\ V_{\mathrm{gap}}$ [m/s] with V_{utna} and V_{UTNb} with $\chi\ V_{\mathrm{gap}}$ (χ is the correction factor of velocity due to turbulent flow in slide-gate region, as explained elsewhere[2]). Additionally, L_{Up} and L_{UTN} are changed to L_{USEN} (upper SEN length [m]), and L_{lp} (lower plate length [m]), respectively. Also, D_{UTNa}, D_{UTNb}, D_{slide}, and D_{p} are replaced with D_{slide}, D_{USENa} (upper SEN entry diameter [m]), D_{USENa}, and D_{USENb} (upper SEN exit diameter [m]), respectively. Finally, f_{UTN} is replaced with f_{SEN} (SEN region wall friction factor). In addition to wall friction, there are three more pressure loss terms between points 5 and 6 in the slide gate region.

The next term, $\Delta P_{\mathrm{L,USEN}}$, is pressure loss due to gradual contraction or expansion in the upper SEN region [Pa]. For gradual expansion, the expression is the same as Eq. [18] changing V_{utna} to $\gamma\ V_{\mathrm{gap}}$ and replacing A_{UTNa} with A_{USENa} (upper SEN entry area [m^2]), and A_{UTNb} with A_{USENb} (upper SEN exit area [m^2]). In case of gradual contraction, the expression is the same as Eq. [19] changing V_{utnb} to $\chi\ V_{\mathrm{gap}}$. Also, A_{UTNa} is replaced with A_{USENa} and A_{UTNb} with A_{USENb}.

Next, $\Delta P_{\mathrm{L,gate\_2}}$, pressure loss due to sudden cross section change between upper part of lower plate and slide gate plate [Pa]. For a sudden expansion, the expression is the same as Eq. [20], changing V_{UTNb} to $\chi\ V_{\mathrm{gap}}$. As for the area, A_{UTNb} is replaced with A_{sg}. In case of sudden contraction, the expression is the same as Eq. [21], changing V_{p} to $\chi\ V_{\mathrm{gap}}$, and A_{UTNb} is replaced with A_{sg}.

Finally, $\Delta P_{\mathrm{L,P\_2}}$, pressure loss due to gradual contraction or expansion at transition between lower plate and upper SEN region [Pa], The expression is the same as Eqs. [18] or [19], depending on whether there is gradual expansion or contraction, with appropriate changes in velocity. For gradual expansion changing V_{utnb} is changed to V_{p} (fluid velocity in lower/upper plate slide-gate region [m/s]), and A_{UTNa} is replaced with A_{USENa}, and A_{UTNa} with A_{p}. In case of gradual contraction, V_{utnb} changed to V_{USENa} (fluid velocity in upper SEN region [m/s]) and A_{UTNa} replaced with A_{p} and A_{UTNb} changed to A_{USENa}.

6. *Lower SEN tapered region (points 6 to 7)*

Two pressure loss terms are present in this region. $\Delta P_{\mathrm{Lf,6-7}}$ is the wall friction between points 6 and 7 [Pa], similar to Eq. [22] with appropriate changes in velocity, V_{p} to V_{USENb} [m/s], and replacing h_{4-5} with h_{6-7} (tapered SEN length [m]). Additionally, D_{slide}, and D_{p} are changed to D_{USENa} (upper SEN entry diameter [m]) and D_{USENb} (upper SEN exit diameter [m]). Finally, f_{UTN} is replaced with f_{SEN} (SEN region wall friction factor).

Secondly, there is a pressure loss caused by possible taper in the tapered region of the lower SEN, $P_{\mathrm{L,tap}}$ which is the same as Eqs. [18] or [19] with appropriate changes in velocity, V_{utnb} to χV_{gap} or V_{utna} to V_{SEN} (in case of gradual contraction or expansion, respectively). For gradual expansion, A_{UTNb} is replaced with A_{SEN} as SEN exit area [m^2], and A_{UTNa} with A_{USENb}. In case of gradual contraction, A_{UTNa} is replaced with A_{USENb} and A_{UTNb} with A_{SEN}.

7. *Lower SEN to port region (points 7 to 8)*

Assuming that the lower SEN is straight below the potentially-tapered region, the only pressure loss term between points 7 and 8 is due to wall friction[28]:

$$\Delta P_{\mathrm{L,f7-8}} = \frac{1}{2}\rho_{\mathrm{m}} f_{\mathrm{SEN}} (V_{\mathrm{SEN}})^2 \frac{h_{7-8}}{D_{\mathrm{SEN}}} \qquad [26]$$

where $P_{\mathrm{L,f7-8}}$ is the pressure loss due to wall friction [Pa], f_{SEN} is the SEN wall friction factor, V_{SEN} liquid velocity at lower SEN region [m/s], h_{7-8} in the height difference between points 7 and 8 [m], and f_{SEN} is the friction factor in the SEN region. Note that a beaver tail nozzle, often used in thin-slab casting, can be simulated with a long tapered upper SEN and a short lower SEN (between points 7 and 8) with larger diameter.

8. *Port region (points 8 to 9)*

In the port region, between points 8 and 9, there are three pressure loss terms: $\Delta P_{\mathrm{L,port}}, \Delta P_{\mathrm{L,tee}}$, and $\Delta P_{\mathrm{C,port}}$. The first pressure loss, $\Delta P_{\mathrm{L,port}}$, is due to sudden contraction between the lower SEN and the port [Pa], and is defined as:[2]

$$\begin{cases} \Delta P_{\mathrm{L,port}} = \frac{1}{2}\rho_{\mathrm{m}} {V_{\mathrm{SEN}}}^2 \left(\frac{A_{\mathrm{SEN}}}{2A_{\mathrm{port}}} - 1\right)^2 & A_{\mathrm{SEN}} > 2A_{\mathrm{port}} \\ \Delta P_{\mathrm{L,port}} = 0 & A_{\mathrm{SEN}} \le 2A_{\mathrm{port}} \end{cases} \qquad [27]$$

where V_{SEN} is fluid velocity through the lower SEN region [m/s], A_{SEN} is lower SEN area [m^2], and A_{port} is port cross-section area [m^2].

The second pressure drop is due to the change of flow direction[2] [Pa], and is defined as:

$$\Delta P_{\mathrm{L,tee}} = \frac{1}{2}\rho_{\mathrm{m}} K {V_{\mathrm{SEN}}}^2 \qquad [28]$$

where V_{SEN} is fluid velocity through lower SEN region [m/s], and K is the port loss constant, which can be input in the Settings menu, and defaults to 0.2.[2]

The third pressure loss in the port region is due to clogging:

$$\Delta P_{\mathrm{C,port}} = \frac{1}{2}\rho_{\mathrm{m}} C_{\mathrm{port}} {V_{\mathrm{port}}}^2 \qquad [29]$$

where V_{port} is fluid velocity through the port [m/s], and C_{port} is the port clogging constant, which can be input (in the Settings menu) or left blank (to default to 1).

D. *Incorporation of Clogging*

As shown in Figure 2, possible clogging can be defined at several different places. For the slide gate and port regions, a clogging coefficient is considered (Eqs. [23] and [29]). However, for other portions (tundish floor opening, UTN, lower/upper plate, upper SEN, tapered SEN, and lower SEN), clogging is given in terms of a specified reduction in the diameter of that nozzle portion. For example, if the original diameter of UTN is as 80 mm, 1 mm of clogging, ($C = 1$mm), would reduce the diameter to 80 − 2 = 78 mm:

$$D_{\mathrm{C,UTN}} = D_{\mathrm{UTN}} \pm 2\, C_{\mathrm{UTN}} \qquad [30]$$

Additionally, for portions where the user inputs the area and perimeter, first the equivalent ellipse is constructed with major and minor axes calculated as follows:

$$2a = 4A\sqrt{\frac{1}{P^2 - \sqrt{P^4 - 16\pi^2 A^2}}} \qquad [31]$$

$$2b = \frac{2A}{\pi a} \qquad [32]$$

where $2a,\ 2b,\ A$, and P are major axis, minor axis, area, and simplified perimeter of the portion, respectively.[31]

Then, the amount of clogging is subtracted (for positive clogging) or added (for negative clogging) to the equivalent major and minor axis, according to Eq. [30]. Next, the clogged area and perimeter of the ellipse is calculated from the new major and minor axis lengths:

$$A_C = \pi a_C b_C \quad [33]$$

$$P_C = 2\pi\sqrt{\frac{a_C{}^2 + b_C{}^2}{2}} \quad [34]$$

Finally, the equivalent hydraulic diameter for further calculations is obtained by the following:

$$D_{H,C} = \frac{4A_C}{P_C} \quad [35]$$

It is important to note that the new model can accurately simulate the effects of any of the different types of clogging (such as aspiration, inclusion deposit, steel solidification skulling, *etc.*) on flow rate and pressure inside the nozzle flow-control system, so long as the shape and location of the clog is known. Although the effects of any clog type can be calculated, however, the focus of the PFSG model and the work done by Yang *et al.*[2] is on the aspiration-type clogging. These models can even quantify the aspiration rate for such clogging.[2] The prediction of other types of clogging is beyond the capability of the current model, but is certainly worthy of investigation in future work.

E. *Slide Gate Opening Definitions/Relations*

Four different popular definitions of the slide gate opening, shown in Figure 4, are considered in the PFSG modeling package. Note that in PFSG, the lower and upper plate diameter are considered equal, D_p, and also match the, D_{USENa}, while the hole in the middle plate, D_{slide}, can be smaller.

1. *Linear slide gate opening*

The linear slide gate opening, f_L, is defined as:

$$f_L = \frac{L}{D_{slide}} \quad [36]$$

where D_{slide} is the middle-plate hole diameter [m] and L is the gap opening length [m], (Figure 4(b)). It ranges from zero (closed), when $L = 0$, to 100 pct (fully open), when $L = D_{slide}$. For any position, the gap opening distance L is the maximum distance from the left side of the nozzle bore (lower/upper plate hole diameter) to the right side of the circular opening in the sliding gate plate. Note if the middle plate hole is smaller than the nozzle bore then there is still some flow restriction even when the slide gate is 100 pct open.

2. *Plant (offset) linear opening fraction*

The plant slide-gate opening, f_p, is defined[1] by specifying the distance E [m] and the distance to the reference line, E_{max} [m], which is offset (relative to f_L) from the left side of the nozzle bore by the distance ($E_{max} - D_{USENa}$), and is expressed as:

$$f_p = \frac{E}{E_{max}} \quad [37]$$

This common situation occurs when the reference line for $E = 0$ does not match with the left edge of the nozzle bore diameter (Figure 4). For this situation of an offset, the gap opening ranges from zero (when $E = E_{max} - D_{USENa}$) to fully open (when $E = E_{max}$).

3. *Area fraction*

The area-based gate opening, f_A, is defined by:

$$f_A = \frac{A_{gap}}{A_{Bore}} \quad [38]$$

where A_{gap} is the area of the gap opening (black shaded region in Figure 4(b)) in [m^2] and A_{Bore} is the area of the lower plate hole [m^2].

4. *Center to center distance*

Another way to define the slide-gate opening used in some plants is Center-to-Center distance, *CTC* [m]. This measure of opening is simply the distance between the two centerlines of the nozzle bore (lower plate opening) and the slide-gate opening. A given *CTC* value can be converted to f_L as follows:

$$f_L = \frac{\left(\frac{\left(D_{slide} + D_p\right)}{2} - CTC\right)}{D_{slide}} \quad [39]$$

5. *Implementation*

The user typically inputs f_L and E_{max}, and PFSG then outputs all of the results, including those based on the second and third definitions, f_p and f_A. In case f_L is left blank and both E and E_{max} are also unknown, PFSG first calculates f_L based on the rest of the casting conditions. Then assuming $E_{max} = D_{USENa}$, (no offset), PFSG calculates E according to Eq. [41]. Alternatively, if f_L is left blank and both E and E_{max} are input, then PFSG calculates f_p and uses it to find and output f_L (Eq. [41]). If f_p is input and either E or E_{max} are left blank, then PFSG outputs the missing value (E or E_{max}) in addition to f_L. If both E and E_{max} are missing, then f_p is assumed equal to $f_L(D_{slide}/D_{USENa})$, meaning $E = L$ and $E_{max} = D_{USENa}$ and there is no offset.

The relationship between f_p and f_L is:

$$f_p = \frac{f_L D}{E_{max}} + \frac{Offset}{E_{max}} \quad [40]$$

where the offset distance is related to E, f_L, D, E_{max}, and D_{USENa} as follows:

$$\text{Offset} = E - f_L D = E_{max} - D_{USENa} \quad [41]$$

$$D = \min(D_{slide}, D_{USENa}) \quad [42]$$

The plant offset method with f_p is useful for model calibration, if there is uncertainty regarding the location of the reference line in the plant relative to the edge of the nozzle bore. Note that the user can input linear opening distance (instead of linear opening fraction), as a special case of f_p simply by setting E_{max} to D_p, and inputting E, which will then become the same as L. Beware that one of E, E_{max}, and f_L must be left blank, or the gap opening is over constrained and the program will give an error message if the 3 inputs are not compatible.

F. *Model Solution Procedure*

The 10 pressure energy equations,[2] Eq. [1], are solved simultaneously, in a fully-coupled manner, for the user-specified unknowns using the implicit FSOLVE subroutine in MATLAB.[26] This equation solver aims to minimize the error in the total energy balance, which is the difference between pressure at point 2 (bottom of the tundish) and the hydrostatic pressure calculated at the tundish bottom, which is the maximum pressure in the system. This difference is equal to pressure at point 1 (molten steel surface in tundish). Therefore, FSOLVE iterates to minimize the pressure at point 1 to be as close as possible to zero gauge pressure. After convergence, the solution error is only about 10^{-12} kJ/m^3 (10^{-10} pct). The entire model runs in less than 10 seconds on a personal computer and typical converges to within 10^{-3} kJ/m^3 error in energy balance. Finally, if the user specifies all inputs, then the model simply solves for the error in the energy balance, which does not require iteration with FSOLVE, and runs in only a few seconds.

G. *PFSG Inputs and Outputs*

Input data for the PFSG model includes the nozzle geometry (dimensions) and casting conditions. Several examples for cases studied in this work are given in Table I, including the Standard nozzle, used at the former Inland Steel caster, and studied in previous work.[1]

Conditions (input data) for the Standard nozzle case are also shown in Figure 2.

The PFSG model assumes that upon injection into the nozzle, argon gas heats instantly to 1823 K, according to previous work.[32] The dynamic viscosity of the fluid is set at 0.001 Pa·s for water and 0.0063 Pa·s for molten steel. Finally, standard STP conditions, for gas injection, are P_{atm} = 101 kPa and T_{amb} = 298 K.

The first output of PFSG, shown in Figure 3(a), is the gauge pressure distribution plot down the 10 different points in the tundish, UTN, SEN, and mold, arranged according to vertical distance. Next is a plot of flow rate in the system predicted as a function of slide-gate opening, for all three definitions of the opening (Figure 3(b)).

Figure 4(a) shows the third output plot: the relation between linear slide-gate opening fraction (f_L), slide-gate area-opening fraction, (f_A) and plant offset linear opening fraction (f_p) for the given E and E_{max}. If E and E_{max} are both omitted, then E_{max} is set to D_{USENa} (offset distance = 0), so the plant offset linear fraction then coincides with the linear slide-gate opening fraction

Table I. Nozzle Dimensions and Plant Casting Conditions Studied in This Work

Dimension/Condition	Standard Nozzle	Nozzle 1	Nozzle 2	Nozzle 3	Nozzle 4
UTN Entry Diameter [mm]	114	80	111	81	30
UTN Length [mm]	241.5	255	280	254	188.5
Upper Plate Thickness [mm]	63	50	25	50	14
UTN Exit Diameter [mm]	78	80	70	78	30
Middle Sliding Plate Thickness [mm]	63	25	40.5	35	17
Middle Sliding Plate Hole Diameter [mm]	78	80	70	80	30
Lower Plate Thickness [mm]	100	160	35	160	14
SEN Bore Diameter [mm]	78	75	72.73	85	30
SEN Length [mm]	748	714	776	709	327
Port Height [mm]	78	81	82.75	80	28.5
Port Area [mm^2]	5625	4800	6392.2	4493.1	812.3
Port Angle (Down) [deg]	15	15	15	15	25
Slide-Gate Opening f_L [Pct]	32.4	40.2	57.9	43.2	47.0
Tundish Height h_{TUN} [mm]	1000	1040	1004 (PFSG.V.3.2)	927.2 (PFSG.V.3.2)	370
Casting Speed V_c [m/min]	0.8	0.60	1.3	0.6	0.92
Argon Gas Flow Rate [SLPM]	10	6	6	0	0
Submergence Depth [mm]	200	210	110	180	60
Slab Width [mm] × Thickness [mm]	1321 × 203.2	1900 × 300	1384 × 235	2300 × 300	500 × 75
Fluid Density [kg/m^3]	7000	7000	7000	7000	1000
Transition Reynolds Number[28]	4000	4000	4000	4000	4000
Clogging	0 (everywhere)	0 (everywhere)	0 (everywhere)	0 (everywhere)	0 (everywhere)

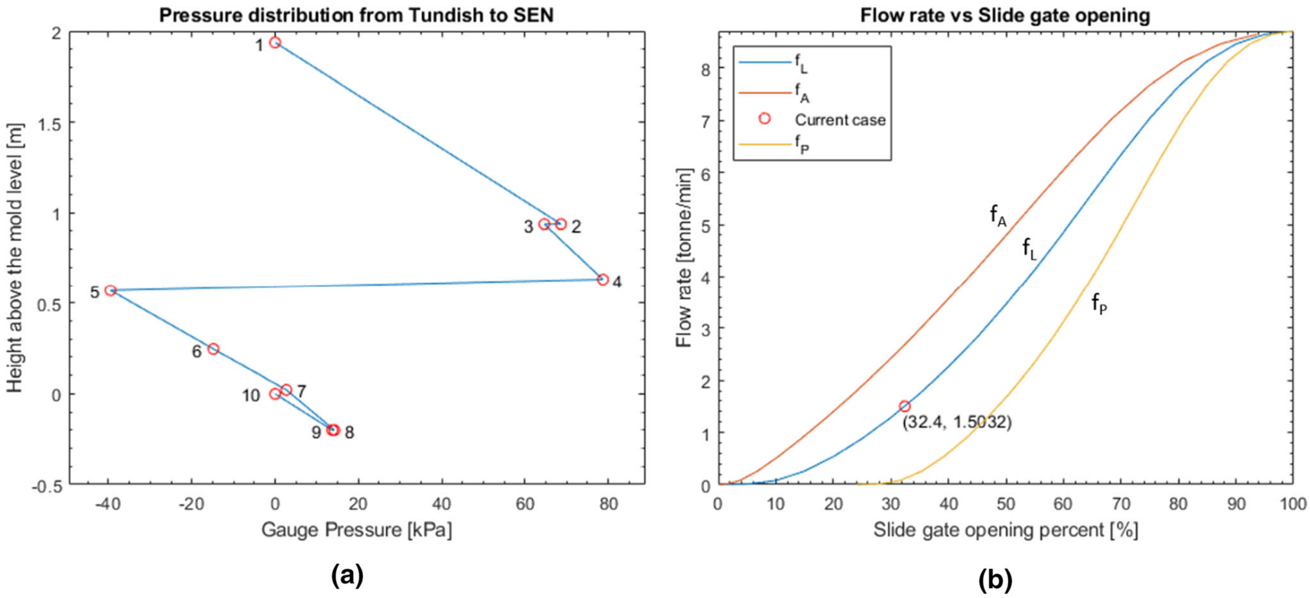

Fig. 3—Results for Standard nozzle (PFSG V.3.2) (*a*) pressure distribution, (*b*) flow rate for different definitions of gate opening.

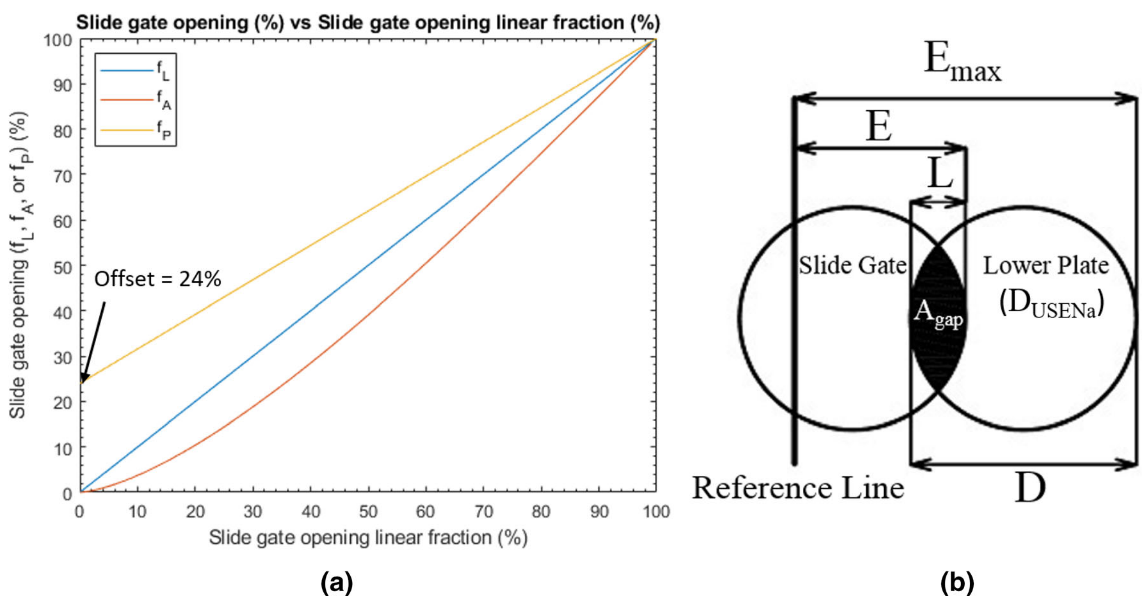

Fig. 4—(*a*) Relationship between f_p, f_L, and f_A (*b*) geometrical relationship between parameters in calculating f_L and f_p for Standard nozzle ($D_{slide} = D_{USENa}$).

(Figure 4). Finally, PFSG outputs the error in the energy balance [kJ/m^3] for the conditions specified, which should be nearly zero, *i.e.* < 0.1 kJ/m^3, if the input data is compatible. (Figure 2).

An important feature of the PFSG program is its ability to conduct parametric studies, in which the effect of changing one or more casting condition(s) or geometrical input(s) on the pressure distribution/flow rate can be studied. In addition, the program can also be used as an inverse model to determine the value of one unknown casting condition, given all of the other inputs (casting conditions and geometric data. This feature is particularly useful for researchers, process engineers, and other professionals in the steel industry to calibrate the model for a given plant, and then to apply it to solve problems and to gain deeper insights into the pressure and flow-related phenomena that affect continuous casting of steel.

The first version of PFSG was basically a user-friendly version of the model by Yang *et al.*[2] in which the inverse-capability of parametric study was added. PFSG V.1 also generated the three graphs and output file of useful information. Later versions of PFSG added features to this model. PFSG V.2.2 added FSOLVE, the Settings menu to customize clogging at different places inside the nozzle, absolute roughness in UTN and

SEN, pressure loss constant at slide gate region and port, fluid density (in case the water model is required to be analyzed), number of nozzles exiting the tundish bottom, and the transition Reynolds number for turbulence.

Finally, PFSG V.3.2 implemented variable argon gas flow rate inside the UTN, slide gate, and SEN according to the local pressures when solving Eq. [4]. It also implemented an improved iteration method. This enabled incorporating the mixture density, which is highly coupled, and thus improved the model accuracy over PFSG V.2.2, which simply assumed constant density, based on the liquid phase. This version also generalized the inverse modeling feature. The value of any one of 6 missing casting conditions (Main window) or any one of 8 missing Clogging values or the Slide Gate Pressure Drop Constant (Settings Menu) may be left blank (unknown) (Figure 2) and solved by PFSG.

III. MODEL VERIFICATION AND VALIDATION

In order to validate and verify the pressure energy model (PFSG), flow rate and pressure distribution prediction of the model is compared with CFD simulations and with available data from plant measurements and water model experiments. The information regarding validation nozzles are given in Table I. Please note that two different versions of PFSG are used: PFSG V.2.2 (which assumes constant argon gas expansion) and PFSG V.3.2 (which considers argon gas expansion varying with position in the nozzle according to the local pressure).

A. *Verification of PFSG with CFD Simulations*

A three-dimensional finite-volume CFD model was applied to predict velocity and pressure fields in the nozzles during continuous casting, for both the real steel caster and water model cases. Velocity and pressure of the turbulent fluid flow inside the Eulerian domain, consisting of the UTN, slide gate, and SEN nozzle interiors, were calculated using a Reynolds-Averaged Navier–Stokes (RANS) standard k–ε model for steady-state flow or a Large Eddy Simulation (LES) model for transient flow. These new CFD model predictions were compared with PFSG model calculations, as well as plant and water model measurements when available.

The continuity equation for mass conservation is:

$$\frac{\partial}{\partial x_i}(\rho u_i) = 0 \qquad [43]$$

where ρ is fluid density [kg/m^3] and u_i is velocity in the 3 coordinate directions [m/s]. The Navier–Stokes equation for momentum conservation is:

$$\frac{\partial}{\partial t}(\rho u_i) + \frac{\partial}{\partial x_j}(\rho u_i u_j) = -\frac{\partial p^*}{\partial x_i} + \frac{\partial}{\partial x_j}\left[(\mu + \mu_t)\left(\frac{\partial u_i}{\partial x_j} + \frac{\partial u_j}{\partial x_i}\right)\right] \qquad [44]$$

where p^* is modified pressure ($p^* = p + \frac{2}{3}\rho k_r$) [Pa], p is gauge static pressure [Pa], k_r is an unknown residual kinetic energy, μ is dynamic viscosity of the fluid [Pa·s], and μ_t is turbulent viscosity [Pa·s] which is calculated from two additional scalar transport equations,[33] of turbulent kinetic energy (k) and its dissipation rate (ε), or from the Smagorinsky–Lilly subgrid-scale viscosity model.[34] To consider argon gas injection in the CFD models, the two-phase Eulerian-Eulerian model is implemented into the RANS model, which solves two sets of mass and momentum equations for the liquid and gas phases.[35] A Discrete Phase Model (DPM) is two-way coupled with the LES fluid flow model, by including a source term into the momentum equation, and solving an additional transport equation for each gas bubble, as explained elsewhere.[36]

For boundary conditions, inlet area at the top of the UTN (tundish bottom) was assigned as a constant-velocity inlet. The nozzle port outlets were assigned as a pressure outlet according to the hydrostatic pressure head distance from the nozzle ports to the top surface level in the mold. Nozzle walls were given standard wall functions in the RANS model, and a wall function approach given by Werner and Wengle[37] in the LES model. The initial condition was zero velocity everywhere. The equations were discretized with hexahedral finite-volume cells (eg. Nozzle 3 case: ~ 20,000 cells in the RANS model and ~ 150,000 cells in the LES model), and solved for velocity and pressure by the Semi-Implicit Pressure Linked Equations (SIMPLE) algorithm, using the CFD package, Ansys Fluent.[35] Convergence of the steady-state RANS model was defined when all scaled residuals were stably lower than 10^{-4}. The transient LES model was started at time = 0 second and run for 7 seconds. First, the flow was allowed to develop for 1 second, which is longer than the residence time of molten steel inside the nozzle (total nozzle length/average velocity: 1.2 m/1.3 m/s = 0.9 second). Then, the LES simulation was run 6 seconds further to calculate time-averages of the velocity and pressure fields.

B. *Validation of PFSG with Inland Steel Plant Data*

Using the experimental data (curve fit of plant data) provided by Inland Steel,[1] the slide-gate opening flow rate relation for Standard nozzle conditions (Table I) is plotted and compared in Figure 5(a) with the PFSG V.2.2 and PFSG V.3.2 model predictions, and with previous RANS simulations done with CFX by Bai *et al.*[1] The corresponding pressure distribution is plotted in Figure 5(b) using both versions of PFSG.

As shown in Figure 5(a), the predicted relation between steel flow rate and slide-gate opening matches well with both plant measurements and the previous CFX predictions.[1] More specifically, the maximum error associated with both PFSG versions and the CFX simulations is around 6 pct, using the plant slide gate opening with 24 pct offset from Bai[1]. These results

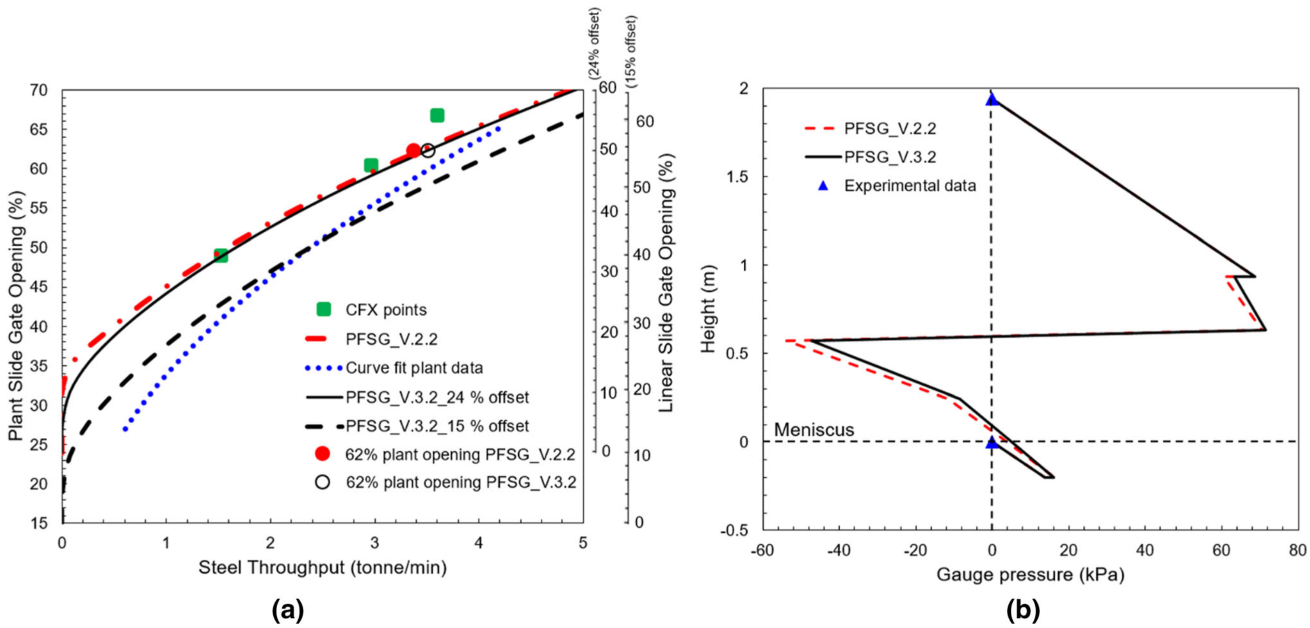

Fig. 5—PFSG model validation with Inland Steel caster data[1] for Standard nozzle casting conditions (*a*) flow rate, (*b*) pressure distribution.

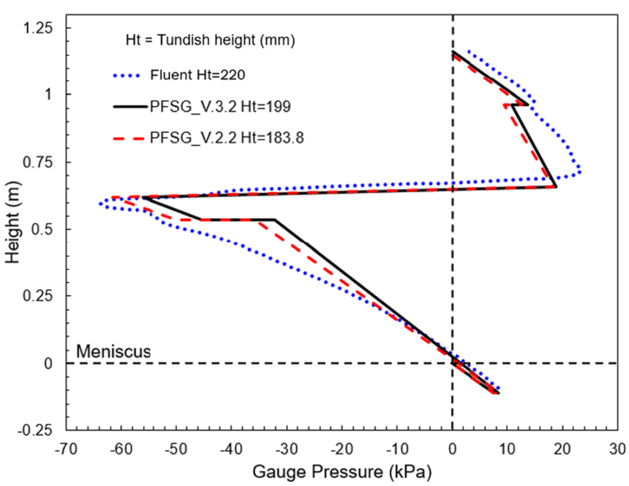

Fig. 6—Pressure distributions verification of PFSG with CFD simulation for Nozzle 2 conditions at 57.85 pct f_L.

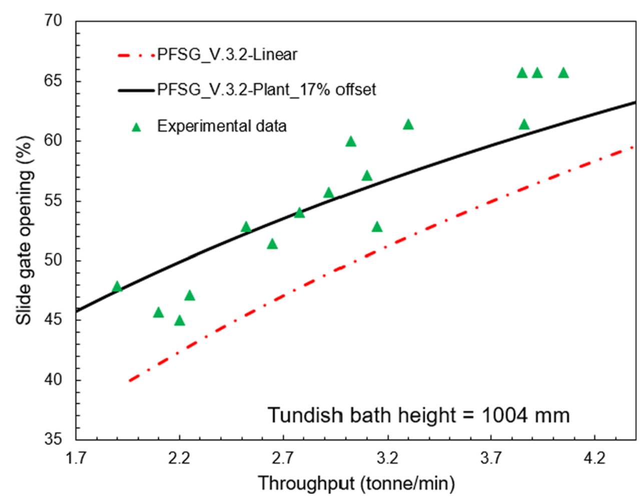

Fig. 7—PFSG V.3.2 validation with Plant 2 data[38] for Nozzle 2 casting conditions.

match the upper range of the plant measurements. Decreasing the offset to 15 pct enables a closer match of PFSG with the best-fit line through the plant data.

Pressure distributions for f_p = 62 pct plant slide-gate opening are plotted in Figure 5(b). The pressure gradient predicted in the nozzles by PFSG V.3.2 is slightly lower than that of PFSG V2.2, due to the argon gas expansion and the lower density of the fluid mixture.

C. *Verification and Validation of PFSG with Plant 2 Data*

Next, the PFSG models were verified with new CFD k-ε RANS simulations and validated with plant measurements at Plant 2 for the conditions and geometry of Nozzle 2 given in Table I. The pressure distributions for 57.85 pct linear slide-gate opening with both PFSG V.3.2 and PFSG V.2.2 are compared with CFD simulation profiles in Figure 6. There is reasonable agreement between the pressure distributions of the CFD simulation and PFSG, which verifies the new model. PFSG V.3.2 differs only slightly from V.2.2, owing to its varying argon gas expansion according to the local pressure. Therefore, PFSG V.3.2 pressure prediction is expected to be more realistic than the Fluent and PFSG V.2.2 profiles, especially when argon flow rate is higher, so the differences are greater.

Figure 7 compares the predicted relation between flow rate and slide gate opening fraction from PFSG V.3.2 with experimental data from Plant 2.[38] The trends match reasonably well. However, a much better match was obtained using f_p with an offset of 18 mm, compared to that with f_L.

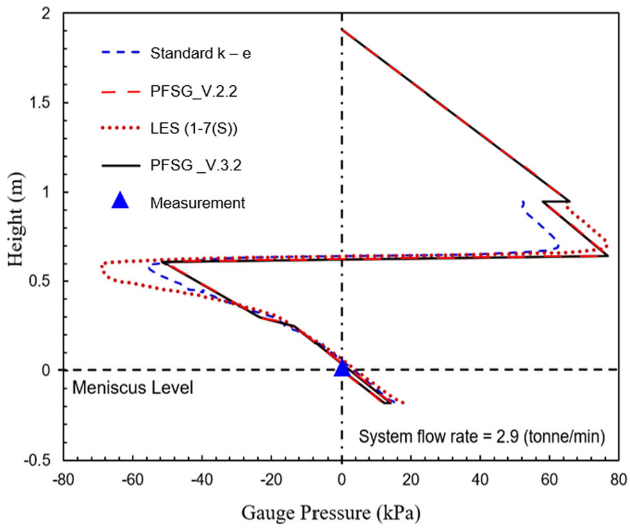

Fig. 8—PFSG verification with Plant 3 Nozzle 3 using CFD simulations.

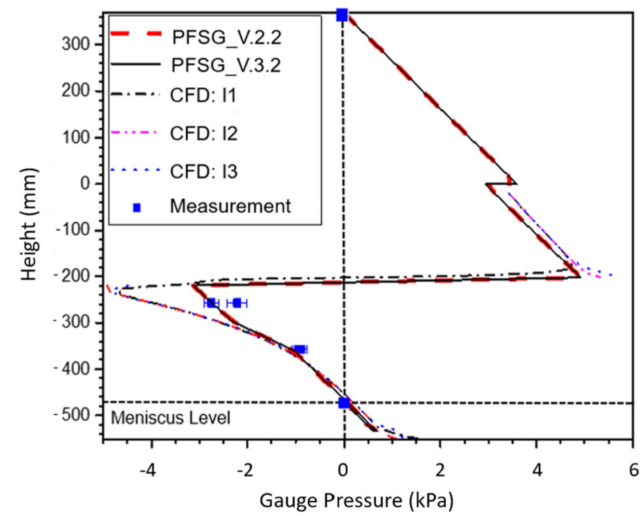

Fig. 9—PFSG model validation with Plant 4 water model data[39] for Nozzle 4 conditions (l_1: center line, l_2: line down front, l_3: line down side of nozzle bore).

D. *Verification of PFSG with Plant 3 Conditions*

Figure 8 shows the pressure distribution for Nozzle 3 (see Table I) for the nozzle geometry and conditions of the steel caster at Plant 3, using new CFD simulations (both standard k–ε RANS and LES) together with profiles from PFSG V.2.2 and PFSG V.3.2. The pressure predictions from PFSG V.2.2 and PFSG V.3.2 match exactly, because there is zero gas injection. In addition, there is reasonable agreement between PFSG and the CFD simulations (standard k–ε and LES). Note that the CFD simulations do not extend into the tundish, to avoid the expense of adding the extra geometry, and because the hydrostatic pressure Eq. [12] is very accurate in this region. The PFSG model matches best with the LES model results for the overall system pressure drop. In the local region near the slide gate, however, the LES model produces a larger local pressure drop than either the RANS or PFSG models.

E. *Verification and Validation of PFSG with Plant 4 Water Model Experimental Data*

Finally, PFSG results are compared with measurements on a 1/3 scale water model of a steel caster at Plant 4. Details of the conditions and geometry are given in Table I for Nozzle 4. Pressure distributions are plotted in Figure 9 using new CFD k-ε RANS simulations, PFSG V.2.2 and PFSG V.3.2 calculations, and also include the experimental pressure measurements. For this case (with water), the slide gate pressure loss constant, ζ, in Eq. [24], in PFSG V.3.2 and PFSG V.2.2 was increased from its standard value of 1 to 2.1 in order to satisfy the energy balance. Note that the PFSG V.2.2 and PFSG V.3.2 calculations exactly match, owing to the lack of gas injection. The results in Figure 9 show that the pressure distributions predicted by PFSG match very well with the pressure measurements below the slide gate, and better than the CFD simulations. The under-prediction of the minimum pressure by the CFD model in the slide-gate region also occurred in the verification cases for Plant 2 and 3. Except in this region, the CFD predictions along three different paths inside the nozzle are almost identical, which justifies the PFSG model assumption that pressure distribution is uniform in the transverse direction across the nozzle. Finally, the PFSG pressure distributions match almost exactly with the measured tundish height.

IV. PARAMETRIC STUDIES

Having verified and validated the PFSG model, it was applied to conduct several different sets of parametric studies to investigate the effects of casting conditions and nozzle geometry on flow rate and minimum pressure in a typical caster with a slide-gate flow-control system. All of the studies in this section are conducted using PFSG V.3.2 with its inverse-modeling capability. The conditions are based on the Nozzle 1 and Standard nozzle geometries and casting conditions in Table I, except as specifically explained, for the parametric study variations.

It is important to note that in order to maintain energy balance in the system (*i.e.* Error < 0.1 kJ/m^3), always two parameters must change together. Often, the slide-gate opening position (fraction) is one of these two parameters.

A. *Effect of Casting Conditions and Nozzle Geometry on Flow Rate*

In this section, the effect of different casting conditions and nozzle geometry on system flow rate are investigated, based on the Nozzle 1 geometry and casting conditions in Table I. Specifically, the effects of changing the argon gas injection rate, lower-SEN diameter, tundish height, and nozzle submergence depth are investigated, either by allowing corresponding

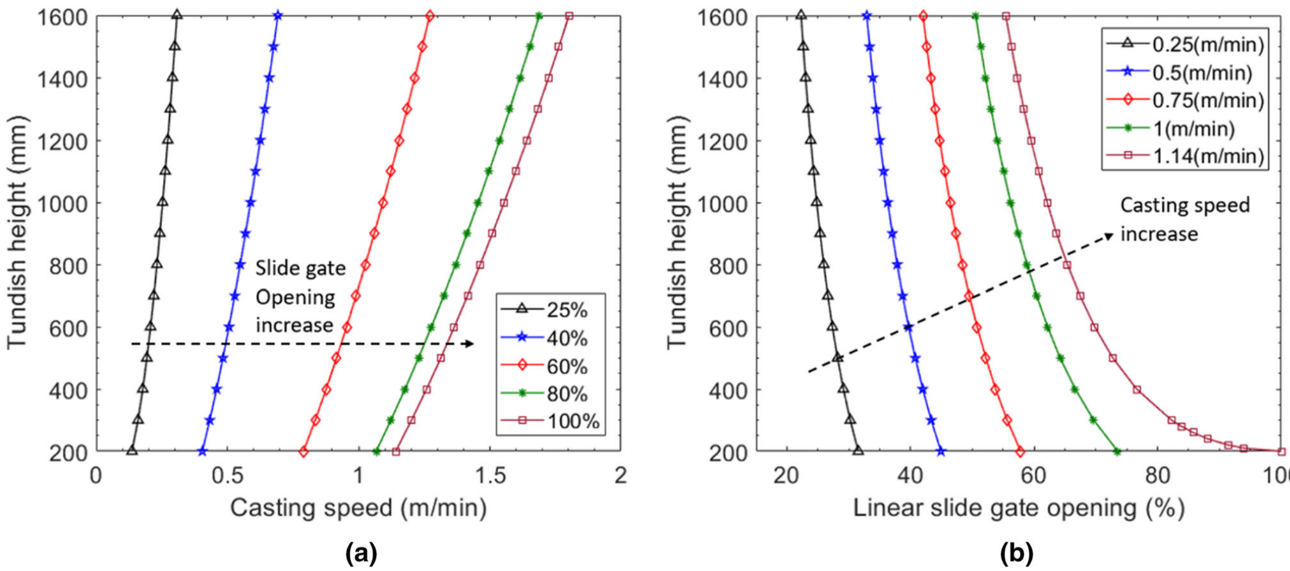

Fig. 10—Relation between tundish height, flow rate (casting speed), and slide-gate opening for Nozzle 1 conditions plotted for (*a*) different slide-gate openings, (*b*) different casting speeds.

changes to the flow rate, or by adjusting the slide-gate opening to maintain the flow rate (and casting speed). The studies begin with an investigation of the relation between tundish height, flow rate, and slide-gate opening position.

1. *Effect of slide-gate opening*

The relationship between tundish height and flow rate (casting speed) depends on the slide-gate opening and is investigated with PFSG as shown in Figure 10. Figure 10(a) quantifies how, for a fixed slide-gate opening, increasing tundish height causes increasing flow and casting speed, due to the increase in the effective head of the system. Also, for a given tundish height, increasing the slide-gate opening causes an increase in flow rate. The same results are presented in Figure 10(b) as the relation between slide-gate opening and tundish height for a given casting speed. To maintain a constant flow rate, as the tundish height drops, the slide-gate opening must increase. The required increase in slide-gate opening is larger at low tundish heights and high casting speeds. The flow rate is most sensitive to small changes in slide-gate opening at high tundish heights and low casting speeds. Finally, Figure 10(b) quantifies how much more the slide gate must open at higher casting speeds.

2. *Effect of Argon gas injection*

Figure 11 illustrates the influence of argon gas injection rate on the steel flow rate for constant tundish height, (1040 m), while adjusting the slide-gate opening. To maintain a given flow rate (casting speed), increasing argon gas injection requires higher slide gate opening. This is because maintaining a constant flow rate with more argon gas means less effective space for the molten steel, which must be compensated by a larger slide gate opening. At a given slide gate opening, increasing the argon gas flow rate would decrease the casting speed

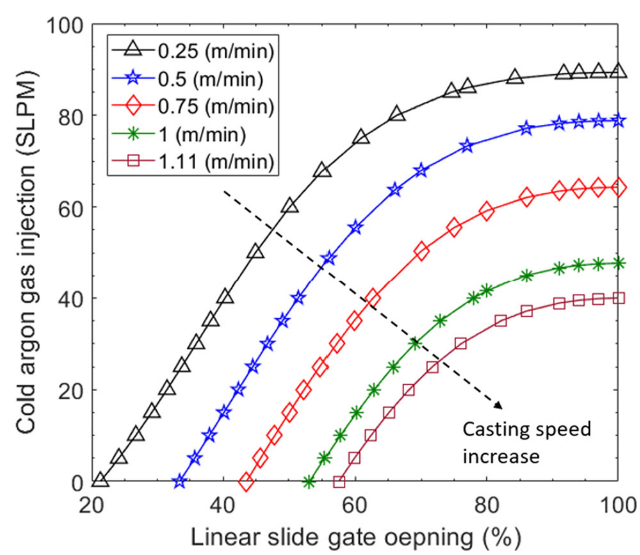

Fig. 11—Effect of casting speed (flow rate) on argon injection rate relation with slide-gate opening for Nozzle 1 conditions.

(flow rate). Finally, for a given argon gas injection rate, increasing slide gate opening naturally causes increased flow rate and casting speed.

3. *Effect of diameter of lower SEN*

To explore the effect of the lower SEN diameter on flow rate, casting speed is plotted in Figure 12 as a function of tundish height for different lower SEN diameters at a fixed slide-gate opening fraction of 40 pct. For a given diameter of the lower SEN, increasing tundish height causes an increase in casting speed, as expected. For a given tundish height, increasing the lower SEN diameter causes a higher flow rate, up to 80 mm which is a straight SEN. Increasing the diameter beyond 80 mm has little effect because the flow resistance of the lower SEN then becomes negligible.

4. *Effect of tundish height*

Figure 12 also shows the effect of tundish height on flow rate/casting speed if the side gate opening remains constant. Submergence depth has the same trend as discussed later.

In actual practice at the plant, increasing tundish height requires decreasing slide-gate opening, to maintain a given steel flow rate, as already presented. These trends are alternatively quantified in Figure 13, which shows the effect of slide-gate opening on casting speed for different liquid levels (heights) in the tundish. This figure shows results for Standard nozzle conditions in Table I, except that the argon flow rate was changed to consider two different values of 0 and 6 SLPM. Increasing tundish height naturally increases the casting speed, for a given slide-gate opening. It is interesting to note that the increase in casting speed is most sensitive to small changes in slide-gate opening when the system is at intermediate gate openings. At extreme low and high slide-gate openings, near to fully opened, and fully closed, the flow rate does not change as much with gate opening. Finally, comparing Figures 13(a) and (b) shows that decreasing the argon gas injection rate (from 6 to 0 SLPM) requires a general decrease in slide-gate opening, with the same general trends. Furthermore, Figure 13(a) shows the theoretical situation that no flow is possible below a certain critical gate opening, due to the argon gas occupying all of the space and leaving no room for molten steel.

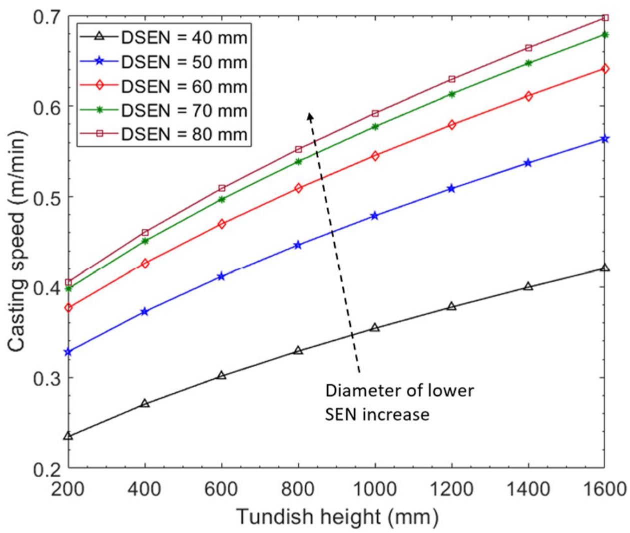

Fig. 12—Effect of diameter of lower SEN on flow rate (casting speed) relation with tundish height for Nozzle 1 conditions (constant 40 pct slide-gate opening).

5. *Effect of submergence depth*

Increasing the submergence depth requires lowering of the entire tundish assembly (for a given nozzle geometry), so the effect is exactly opposite to that of tundish height. As shown in Figure 14, increasing submergence depth for a given slide-gate opening causes a decrease in flow rate and casting speed. Alternatively, increasing submergence depth while maintaining the casting speed requires an increased slide-gate opening. Except at large slide-gate openings, these effects are very small, because the typical range of submergence depths is relatively small (50 to 250 mm). The results are similar when argon gas injection is decreased from 6 SLPM (Figure 14) to zero, except that the slide-gate openings all decrease by ~ 10 to 15 pct, depending on the casting speed. It is important to note that (tundish height − submergence depth) is the fundamental driving force for flow. Therefore, these two variables can be easily combined together into one variable: the difference in liquid level between the tundish and the mold.

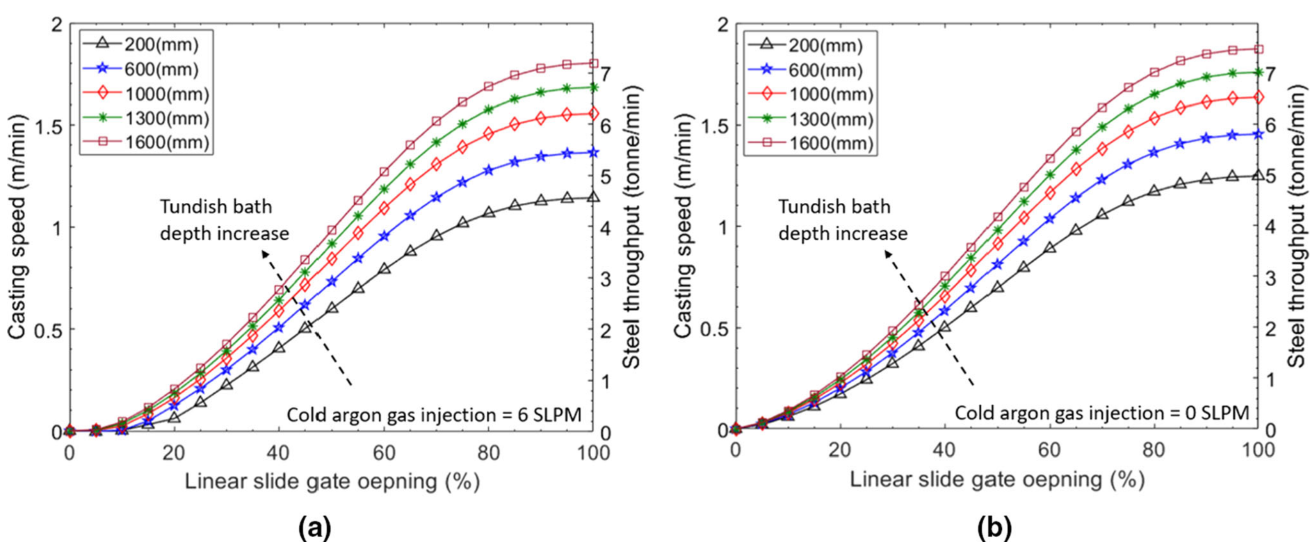

Fig. 13—Effect of tundish height on system flow rate relation with slide-gate opening for Nozzle 1 conditions, with (*a*) 6 SLPM argon gas injection (*b*) 0 argon gas injection.

B. *Minimum Pressure Results*

As explained earlier, the minimum pressure in the flow system occurs just below the slide-gate opening in the upper SEN. Finding the minimum pressure is important, because negative gauge pressure can cause air aspiration, which leads to reoxidation, nozzle clogging and inclusions, resulting in defect(s) in the final product. Therefore, in this section, parametric studies are presented, based on the Standard nozzle and Nozzle 1 geometry and casting conditions in Table I, to investigate the minimum pressure in the nozzle, and to find ways to raise it.

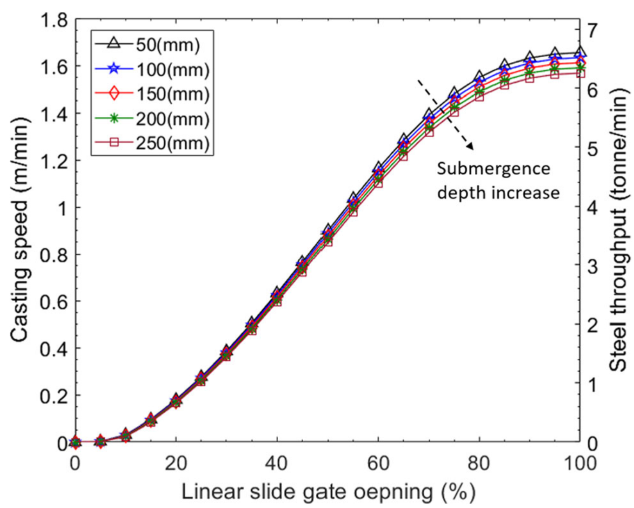

Fig. 14—Effect of nozzle submergence depth on relation between flow rate and slide-gate opening, for Nozzle 1 conditions.

1. *Effects of tundish height and casting speed*

Figures 15 through 17 show the effect of flow rate on minimum pressure at different tundish heights for Standard nozzle conditions, but with three different bore diameters of all of the nozzles (UTN, upper and lower SEN). Increasing casting speed initially causes the minimum pressure to decrease, but after reaching a critical value (minimum of minimums), further increase in casting speed causes the minimum pressure to increase. For a given nozzle bore diameter, the critical minimum pressure is always observed at the same slide-gate opening fraction, regardless of tundish height. Specifically, the minimum pressure occurs at about 50, 70, and 75 pct linear slide-gate opening for nozzle bore diameters of 75, 85, and 90 mm, respectively. The tundish height and SEN submergence depth have a negligible effect on this critical slide-gate opening. Increasing tundish height worsens the minimum negative pressure, as shown in Figures 15(a), 16(a), and 17(a). This finding suggests that to reduce aspiration in the system, tundish height should decrease.

It is worth mentioning that further increase in diameter of the nozzle bores, or excessive increase in tundish height or nozzle length may decrease the minimum pressure to below – 101 kPa in the model. This is not physically possible, so other physics must be activated, such as cavitation and/or non-primed flow, and the current model results are not accurate in such scenarios. This issue is more common in stopper rod systems, as noted in recent work[23] and should be investigated in future studies.

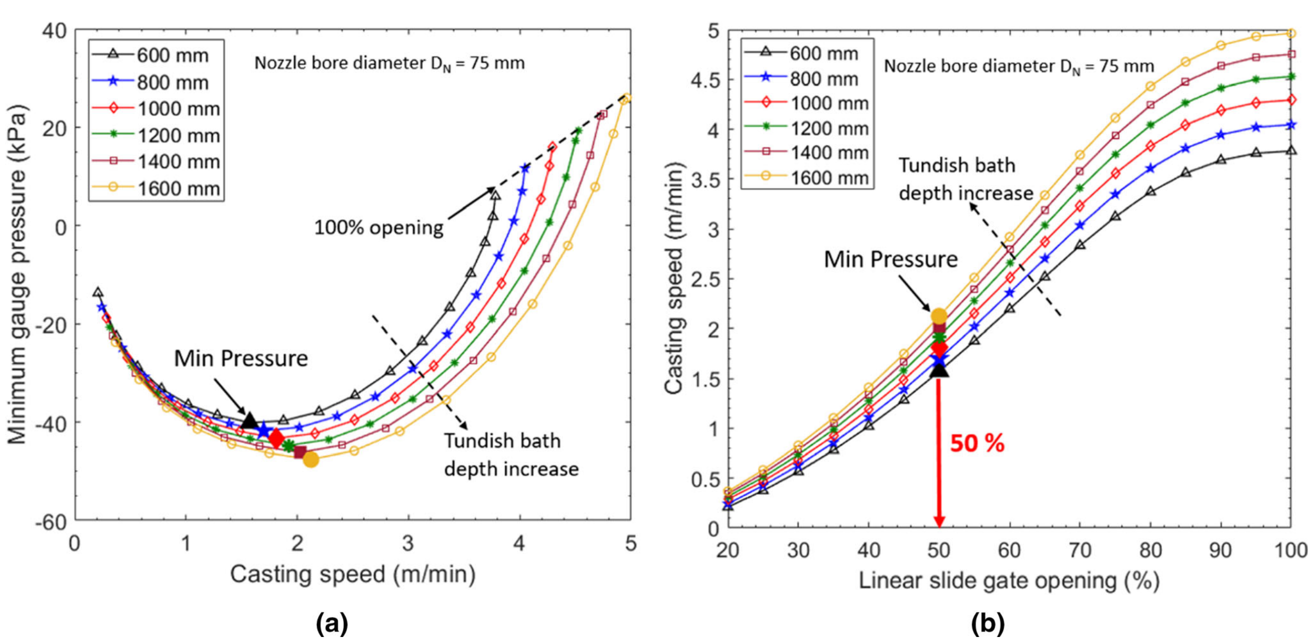

Fig. 15—Effect of tundish height on casting speed relation with (*a*) minimum gauge pressure and (*b*) slide-gate opening (Standard Nozzle conditions but with 75 mm nozzle bore).

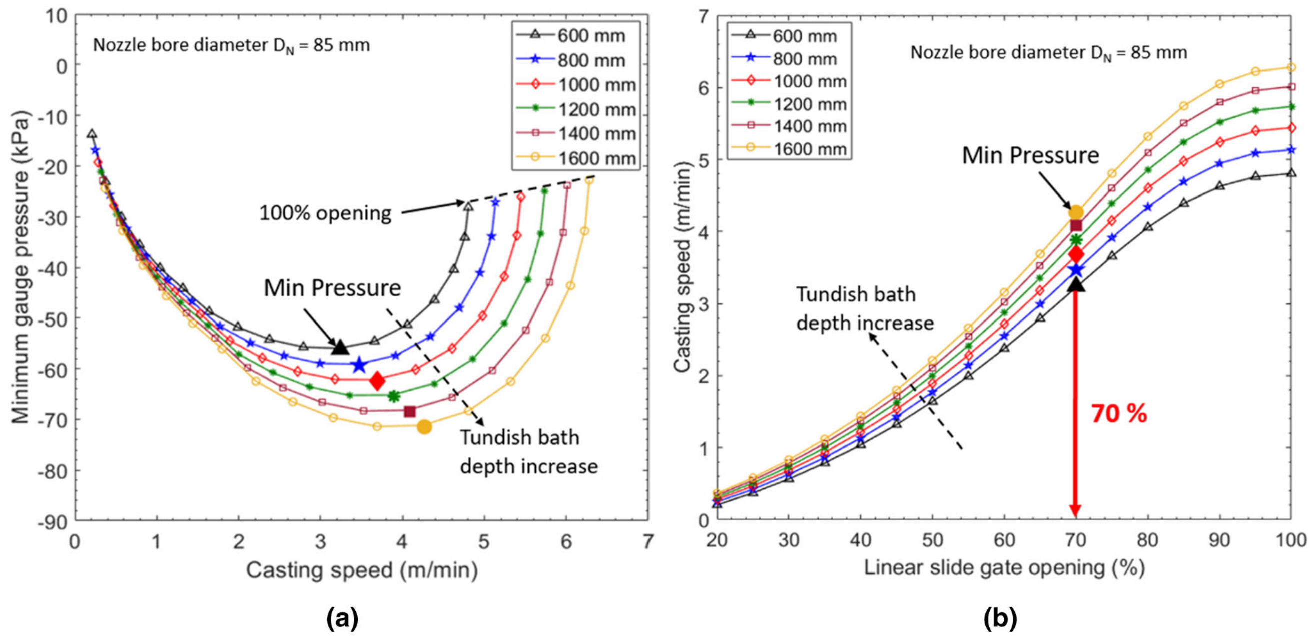

Fig. 16—Effect of tundish height on casting speed relation with (*a*) minimum pressure, (*b*) slide-gate opening (Standard Nozzle conditions but with 85 mm nozzle bore).

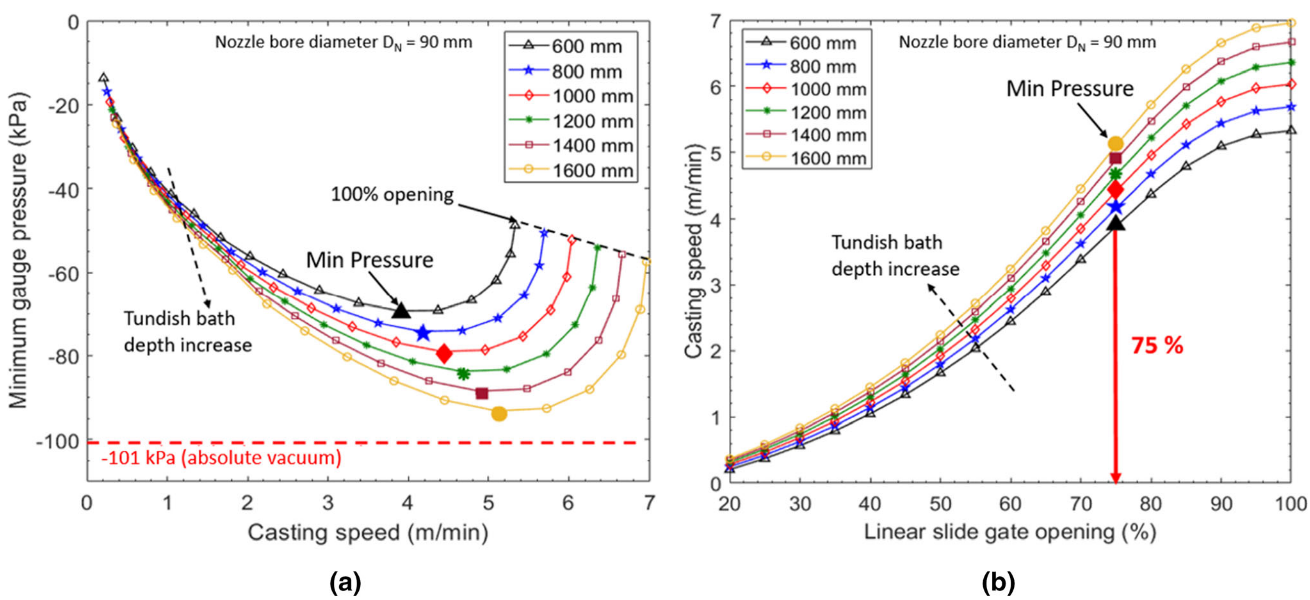

Fig. 17—Effect of tundish height on casting speed relation with (*a*) minimum pressure, (*b*) slide-gate opening (Standard Nozzle conditions but with 90mm nozzle bore).

2. *Effects of submergence depth and casting speed*

The effect of flow rate on minimum pressure in the flow system is plotted with casting speed in Figure 18 for different submergence depths. To maintain the energy balance, the slide-gate opening varies according to the casting speed. The effect is exactly the opposite of the effect of tundish height, as expected. Figure 18(b) shows that the minimum pressure is achieved at a constant linear slide-gate opening (55 pct for this case) regardless of submergence depth. Also, as submergence depth increases, the minimum pressure increases. This is due to the greater slide-gate opening required. These findings suggest that to lessen the negative pressure problem and thereby lessen air aspiration problems, nozzle submergence should be deeper.

3. *Effect of nozzle bore diameter*

The effect of diameter of the lower SEN on the relation between casting speed, tundish height, and minimum pressure can be seen by comparing Figures 15 through 17. In general the trends are the same, and increasing the lower SEN bore diameter causes the

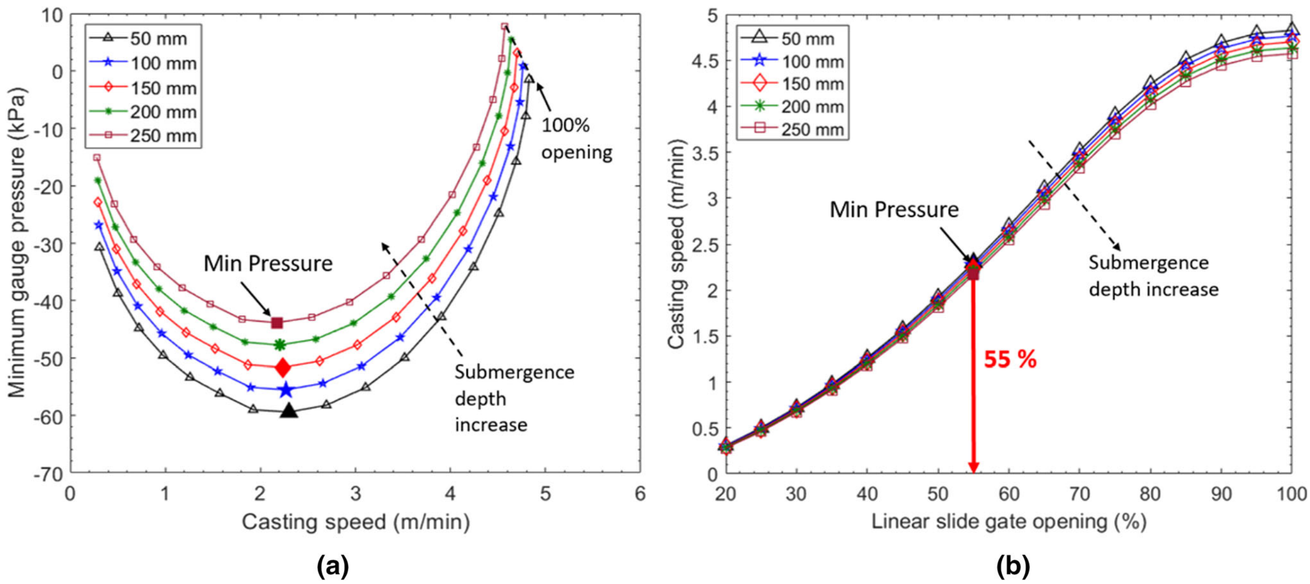

Fig. 18—Effect of nozzle submergence depth on variation of minimum pressure with (*a*) casting speed and (*b*) slide-gate opening. (Standard Nozzle conditions).

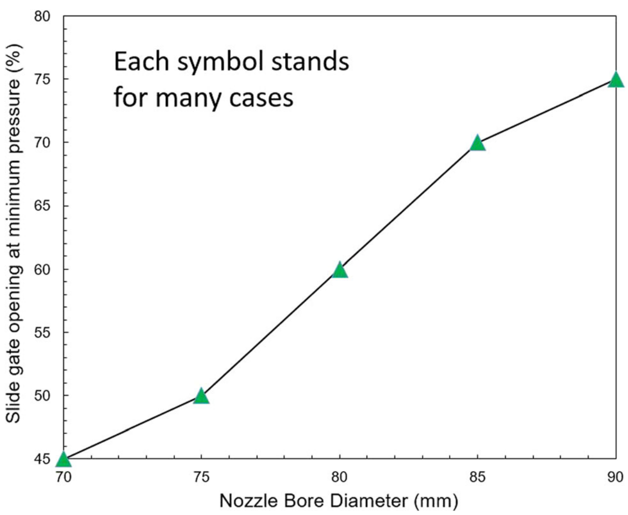

Fig. 19—Effect of lower SEN diameter on slide-gate opening fraction at minimum pressure for Standard nozzle at various casting speeds, tundish heights, and submergence depths.

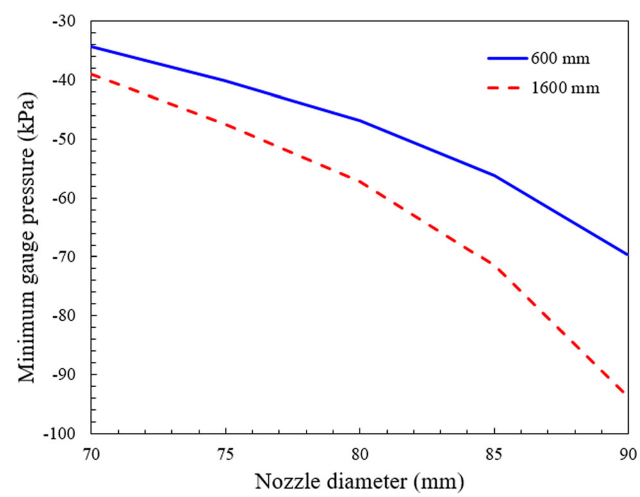

Fig. 20—Effect of diameter of lower SEN on minimum pressure (Standard nozzle).

critical slide-gate opening that causes the lowest minimum pressure to increase, as presented in Section V–B–1. This critical slide-gate opening is almost independent of tundish height, submergence depth, and throughput. However, it increases greatly with increasing bore diameter. This trend is visualized more clearly in Figure 19, where it is important to note that each symbol represents many different cases.

Figure 20 shows the value of the critical (lowest) minimum gauge pressure corresponding to the points in Figure 19, while operating at the critical gate opening that gives minimum pressure. The value of the minimum pressure decreases (gets worse) with increasing tundish height, decreasing submergence depth, or increasing nozzle diameter. In this figure, the casting speed varies from 1.3 m/min (70 mm diameter SEN at tundish height of 600 mm) to 5.2 m/min (90 mm diameter SEN at tundish height of 1600 mm). This finding suggests that air aspiration and reoxidation problems should be minimized with lower tundish level, and/or smaller diameter of the lower SEN, which is consistent with previous findings.[1] Intermediate casting speeds should be avoided, as the minimum pressure is less severe when the slide-gate opening is near to fully opened or fully closed. Unfortunately, this last recommendation requires great care to implement in practice, and many caster operations tend to operate near the worst condition of the critical slide-gate opening.

V. CONCLUSIONS

This work presents a new, standalone, user-friendly MATLAB-based graphical user interface program, Pressure-drop and Flow-rate in Slide Gate systems (PFSG) to quantify pressure distribution and flow rate in continuous steel casting flow-delivery systems. This software tool includes the effects of argon gas with locally-varying expansion with pressure, clogging, and complex nozzle geometry. It can predict potential negative pressure which may cause quality problems related to air aspiration and nozzle clogging. The model is verified with CFD simulations and validated with various plant measurements and water model experiments. The maximum error associated with the validation cases is approximately 6 pct. Parametric studies with the validated model revealed the following results:

- Flow rate and casting speed increase in proportion with increasing the pressure head height that drives the flow, which is governed by the distance between the liquid levels in the tundish and mold.
- Owing to their effects on the pressure head height, the flow rate increases with increasing tundish height, increasing SEN length, and decreasing nozzle submergence depth, for a given slide-gate opening.
- Specifically, doubling the tundish height increases casting speed by about 20 pct, for the same slide-gate opening.
- Varying the nozzle submergence depth over typical commercial caster ranges, between 100 to 200 mm, does not change the flow rate significantly.
- Increasing argon gas injection requires increasing the slide-gate opening to maintain the flow rate.
- Increasing SEN diameter requires decreasing the slide-gate opening (and opening fraction) to maintain flow rate.
- The slide-gate opening fraction at minimum pressure is almost independent of tundish height, submergence depth, and throughput.
- The critical opening fraction at minimum pressure depends greatly on SEN diameter. Specifically, it increases from 45 pct open to 75 pct open with increasing SEN diameter from 70 to 90 mm, for the conditions of this study.
- The effect of argon gas on pressure depends on the slide-gate opening fraction. For large casting speeds, (with large gate openings greater than the critical fraction for minimum pressure), increasing argon injection causes increase in gate opening which increases the minimum pressure, tending to alleviate air aspiration. For small casting speeds, (with small gate openings less than the critical fraction), increasing argon injection causes increasing gate opening, which lowers the minimum pressure and aggravates the air aspiration problem.
- The minimum pressure tends to decrease (gets worse) with increasing tundish level height, and increasing nozzle bore diameter.

ACKNOWLEDGMENTS

The authors thank ArcelorMittal, Baosteel, and POSCO for their assistance in collecting and providing plant data, specifically Dr. Tatha Bhattacharya, ArcelorMittal, Dr. Xiaoming Ruan , Baosteel, and Dr. Shin-Eon Kang, POSCO for help with the plant measurements. Support from the Continuous Casting Center at Colorado School of Mines, and the National Science Foundation GOALI grant (Grant No. CMMI 18-08731) are gratefully acknowledged. Provision of FLUENT licenses through the ANSYS Inc. academic partnership program is also much appreciated. The authors specially thank Dr. Ken Morales, AK Steel, Dirk van der Plas, Tata Steel, Alexandre Dolabella Resende, RHI Magnesita, and Dr. Matthew Zappulla, Colorado School of Mines, for their kind comments and helpful feedback on PFSG.

CONFLICT OF INTEREST

On behalf of all authors, the corresponding author states that there is no conflict of interest.

APPENDIX: WALL FRICTION CALCULATION FOR TAPERED PIPE

Wall friction equation for a pipe with constant diameter (*i.e.* not tapered), discussed in fluid mechanics reference book,[28] is defined as:

$$h = \frac{1}{2} f \frac{L}{D} \frac{V^2}{g} \qquad \text{[A1]}$$

where h is pressure head loss due to wall friction [m], f friction factor, L pipe length [m], D pipe diameter [m], V fluid velocity [m/s], and g Earth's gravitation acceleration [m/s^2].

Now, consider a tapered pipe as shown in Figure A1.

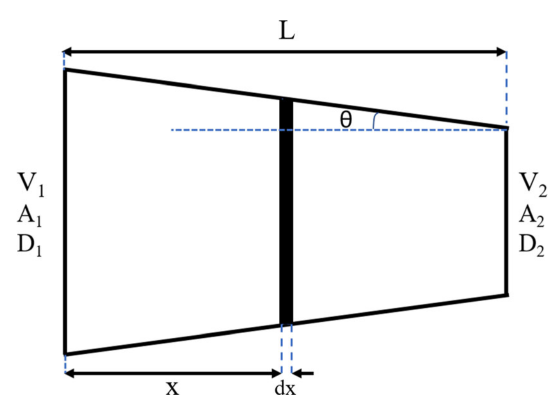

Fig. A1—Schematic of tapered length of nozzle (pipe).

For a very small portion of pipe with the length of dx, it is true to say:

$$\mathrm{d}h = \frac{1}{2} f \frac{\mathrm{d}x}{D} \frac{V^2}{g} \quad \text{[A2]}$$

Consider the continuity equation:

$$V = \frac{V_1 D_1^2}{D^2} \quad \text{[A3]}$$

where V and D are velocity and diameter of the section [m/s] and [m], respectively.

Also from Figure A1:

$$x = \frac{D_1 - D}{2\tan\theta} \quad \text{[A4]}$$

where θ is the taper angle [rad].

Therefore:

$$\mathrm{d}x = \frac{-\mathrm{d}D}{2\tan\theta} \quad \text{[A5]}$$

Substituting Eqs. [A3] and [A5] into Eq. [A2] gives:

$$dh = \frac{1}{2} f \frac{V_1^2 D_1^4}{D^5 g} \frac{-dD}{2\tan\theta} \quad \text{[A6]}$$

Integrating Eq. [A6] over the whole domain (from D_1 to D_2) and simplifying gives:

$$h = \frac{1}{16} \frac{f}{g} \frac{V_1^2}{D_2^4} \frac{\left(D_1^4 - D_2^4\right)}{\tan\theta} \quad \text{[A7]}$$

Insert into Figure A1:

$$\tan\theta = \frac{D_1 - D_2}{2L} \quad \text{[A8]}$$

Finally, substituting Eq. [A8] into Eq. [A7] gives the pressure loss in a tapered pipe due to wall friction:

$$h = \frac{1}{8} f \frac{L}{g} \frac{V_1^2}{D_2^4} (D_1 + D_2)\left(D_1^2 + D_2^2\right) \quad \text{[A9]}$$

REFERENCES

1. H. Bai and B.G. Thomas: *Metall. Trans. B.*, 2001, vol. 32B(4), pp. 707–22.
2. H. Yang, H. Olia, and B.G. Thomas: *Metals.*, 2021, https://doi.org/10.3390/met11010116).
3. L. Zhang, Y. Wang, and X. Zuo: *Metall Trans. B.*, 2008, vol. 39B(4), pp. 534–50.
4. K.G. Rackers and B.G. Thomas: *Proc. of 78th Steelmaking Conf.*, The Iron and Steel Society, Warrendale, PA, vol. 78, 1995, pp. 723–34.
5. S. Yokoya, S. Takagi, H. Souma, M. Iguchi, Y. Asako, and S. Hara: *ISIJ Int.*, 1989, vol. 38, pp. 1346–52.
6. S.M. Cho, S.H. Kim, R. Chaudhary, B.G. Thomas, H.J. Shin, W.R. Choi, and S.K. Kim: *Proc. AISTech,* Indianapolis, IN, AIST, Warrendale, PA, vol. 2, 2011, pp. 669–79.
7. Y. Murakami, S. Kodama, and S. Konuma: *Int. J. Fatigue.*, 1989, vol. 11(5), pp. 291–98.
8. A.D. Wilson: *J. Eng. Mater. Technol.*, 1979, vol. 101 (3), p. 265.
9. L. Zhang, J. Aoki, and B.G. Thomas: *Metall. Trans. B.*, 2006, vol. 37B(3), pp. 361–79.
10. POSCO: Korean Patent Application 10-2012-0026720, 2012.
11. J. Savolainen, A. Rousu, T. Fabritius, O. Mattila, and P. Sulasalmi: *Steel Res. Int.*, 2010, vol. 81, pp. 980–86.
12. R. Liu, B.G. Thomas, J. Sengupta, S.D. Chung, and M. Trinh: *ISIJ Int.*, 2014, vol. 54, pp. 2314–23.
13. M. Javurek, M. Thumfart, and R. Wincor: *Steel Res. Int.*, 2010, vol. 81, pp. 668–74.
14. H. Yang, S.P. Vanka, and B.G. Thomas: *JOM.*, 2018, vol. 70, pp. 2148–56.
15. R. Liu and B.G. Thomas: *Metall. Trans. B.*, 2015, vol. 46(1), pp. 388–405.
16. L. Zhang, S. Yang, K. Cai, J. Li, X. Wan, and B.G. Thomas: *Metall. Trans. B.*, 2007, vol. 38B, pp. 63–83.
17. Y. Wang and L. Zhang: *Metall. Trans. B.*, 2011, vol. 42B, pp. 1319–51.
18. W. Chen, Y. Ren, and L. Zhang: *Steel Res. Int.*, 2019, vol. 90, Article No. 1800287, https://doi.org/10.1002/srin.201800287.
19. B.G. Thomas: *Steel Res. Int.*, 2018, vol. 89, pp. 1–21.
20. H. Yang, S.P. Vanka, and B.G. Thomas: *ISIJ Int.*, 2019, vol. 59, pp. 956–72.
21. S.M. Cho, M. Liang, H. Olia, L. Das, and B.G. Thomas: *TMS Annual Meeting*, Pittsburgh, PA, TMS, Warrendale, PA, 2020, pp. 1161–73, https://doi.org/10.1007/978-3-030-36296-6_108.
22. H. Olia, H. Yang, S.M. Cho, M. Zappulla, and B.G. Thomas: *Proc. AISTech,* AIST, Warrendale, PA, 2020, pp. 1964–74, https://doi.org/10.33313/380/212.
23. R. Liu, B. Forman, H. Yin, and Y. Lee: *Proc. AISTech,* Philadelphia, PA, 2018, vol. 2, pp. 1793–1802.
24. H. Yang, S. Vanka, and B.G. Thomas: *J. Fluids Eng.*, 2018, vol. 140, 101202 (1–12).
25. R. Liu and B.G. Thomas: *Metall. Trans. B.*, 2014, vol. 4B, pp. 388–405.
26. Fsolve: Matlab subroutine from MathWorks Web Resource, https://www.mathworks.com/help/optim/ug/fsolve, accessed 25 July 2021.
27. E.W. Weisstein: Circle–Circle Intersection (From MathWorld—A Wolfram Web Resource), http://mathworld.wolfram.com/Circle-CircleIntersection.html, accessed 29 September 2021.
28. F.M. White: *Fluid Mechanics*, 7th. ed., McGraw Hill, New York, 2011, pp. 356–94.
29. Crane Co.: *Flow of Fluids Through Valves Fittings and Pipes*, Crane Co., New York, 1999, pp. 2-11–2-12.
30. H. Oertel: *Prandtl-Essentials of Fluid Mechanics*, 2nd ed. Springer, New York, 2004, p. 164.
31. G.J.O. Jameson: *Math. Gaz.*, 2014, vol. 98, pp. 227–34.
32. B.G. Thomas and X. Huang: *Metall. Trans. B.*, 1994, vol. 25B, pp. 527–47.
33. B.E. Launder and D.B. Spalding: *Lectures in Mathematical Models of Turbulence*, Academic Press, London, 1972, pp. 157–62.
34. D.K. Lilly: *Phys. Fluids A.*, 1992, vol. 4, pp. 633–35.
35. ANSYS FLUENT 18.1-Theory Guide, ANSYS. Inc., Canonsburg, PA, USA, 2017.
36. S.-M. Cho, S.-H. Kim, and B.G. Thomas: *ISIJ Int.*, 2014, vol. 54, pp. 845–54.
37. H. Werner and H. Wengle: *8th Symp. Turbulent Shear Flows*, Munich, Germany, 1991, pp. 155–68.
38. L. Das and B.G. Thomas: *CCC Annual Meeting*, Continuous Casting Center, Colorado School of Mines, Golden, CO, USA, 15 August 2019.
39. S.-M. Cho and B.G. Thomas: *CCC Annual Meeting*, Continuous Casting Center, Colorado School of Mines, Golden, CO, USA, 15 August 2018.